IEEE Access
Multidisciplinary | Rapid Review | Open Access Journal

Received September 9, 2019, accepted September 24, 2019, date of publication October 14, 2019, date of current version October 28, 2019.

Digital Object Identifier 10.1109/ACCESS.2019.2947407

A Stochastic Channel Model with Dual Mobility for 5G Massive Networks

ALEXANDRE M. PESSOA, IGOR M. GUERREIRO, CARLOS F. M. E. SILVA, TARCISIO F. MACIEL, DIEGO A. SOUSA, DARLAN C. MOREIRA, AND FRANCISCO R. P. CAVALCANTI

Wireless Telecom Research Group (GTEL), Federal University of Ceará (UFC), Fortaleza 60020-181, Brazil

Corresponding author: Alexandre M. Pessoa (alexandrematos@gtel.ufc.br)

This work was supported in part by the Coordenação de Aperfeiçoamento de Pessoal de Nível Superior - Brasil (CAPES) under Grant 001. The work of I. M. Guerreiro was supported by the CNPq under Grant 151004/2017-0.

ABSTRACT In this paper, a new stochastic channel model (SCM) is proposed for fifth-generation (5G) systems. By means of the sum-of-sinusoids (SoS) method to generate spatially consistent random variables (SCRVs), the proposed model extends the 3rd Generation Partnership Project (3GPP)-SCM by considering three important features for accurate simulations in 5G, i.e., support for dual mobility, spatial correlation at both ends of the link and considerable reductions of the required memory consumption when compared with existing models. A typical problem presented in existing channel models, namely the generation of uncorrelated large scale parameters (LSPs) and small scale parameters (SSPs) for close base stations (BSs), is solved, then allowing for more realistic numerical evaluations in most of the 5G scenarios characterized by a large density of BSs and user equipments (UEs) per unit of area, such as ultra-dense networks (UDNs), indoor environments, device-to-device (D2D) and vehicular-to-vehicular (V2V). The proposed model emerges as the first SCM, and therein lower complexity when compared with ray-tracing (RT)-based models, that comprises all the following features: support for single and dual mobility with spatial consistency, smooth time evolution, dynamic modeling, large antenna array, frequency range up 100 GHz and bandwidth up to 2 GHz. Some of the features are calibrated for single mobility in selected scenarios and have shown a good agreement with the calibration results found in the literature.

INDEX TERMS Channel modeling, dual mobility, spatial consistency, low complexity.

I. INTRODUCTION

Recently, a forecast reported by [1] has shown that the number of networked devices around the world will increase from 18 billion in 2017 to 28.5 billion in 2022. Such devices mostly comprise smartphones, laptops, televisions (TVs), Internet of Things (IoT) devices or tablets and are expected to increase the global mobile data traffic sevenfold in this period. To attend the demand for throughput, latency and connectivity request from such devices, the fifth-generation (5G) systems will employ a set of prominent technologies, such as millimetre-wave (mmWave), beamforming and massive multiple-input multiple-output (MIMO) with large bandwidth [2] in a wide range of frequencies (up to 100 GHz) for several different scenarios such as indoor, urban, highway, airports, train stations, etc.

The associate editor coordinating the review of this manuscript and approving it for publication was Jiayi Zhang.

In this context, the set of technologies that will support the 5G systems will require a more realistic representation of the propagation effects which affect radio communication. Some of the main 5G requirements for channel modeling are listed below:

A. Large bandwidth and frequency range

5G channel models should support frequency range from 0.5 GHz to 100 GHz and bandwidths up to 2 GHz. Such requirements, mainly the bandwidth one, will increase substantially the computational complexity since more rays will be needed in order to achieve larger resolutions in both delay and frequency domains.

B. Frequency-dependent parameters

5G channel models should support frequency-dependent parameters such as path loss, building penetration loss (for

outdoor-to-indoor (O2I)), large scale parameters (LSPs) and Doppler effect for diversified environments, such as outdoor-to-outdoor (O2O), indoor, high-speed train, highway, etc.

C. three dimensional (3D) double-directional antennas with massive MIMO

5G channel models should support a full 3D antenna modeling in both transmitter and receiver. Moreover, massive MIMO with spherical wave modeling should also be supported.

D. Smooth time evolution

5G channel models should support smooth time evolution of angles and delays of each ray leading to a dynamic power delay profile (PDP) and power angular profile (PAP) when mobility is supported. Dynamic PAP allows real time beam tracking in mmWave which is one of the 5G key technologies.

E. Dual mobility

5G channel models should support links with dual mobility such as device-to-device (D2D) and vehicular-to-vehicular (V2V). For dual mobility, LSPs and small scale parameters (SSPs) will change as a function of the transmitter and receiver locations causing fast changes in the channel impulse response (CIR) and high Doppler effect.

F. Spatial consistency

The spatial consistency ensures the correlation of LSPs and SSPs for transmitters/receivers when they are close. This requirement is of utmost importance in the context of 5G systems, since its impact on the system performance increases as the density of connected devices per unit of area becomes larger. Spatial consistency demands a high computational complexity, mainly when combined with smooth time evolution and dual mobility links, since the CIR will change as a function of the transmitter and receiver locations.

All the challenges and requirements mentioned above can be achieved using geometry-based models such as ray-tracing (RT) [3], but at the cost of high complexity. Moreover, due to the current growth of the number of devices and cells per unit of area, 5G channel models should also support challenging scenarios such as ultra-dense networks (UDNs) which are typically composed of 100 cells/km^2 and 600 UEs/km^2 [4]. In this context, 5G channel models should not only provide realistic modeling of the propagation effects but also deal with aspects related to computational complexity and management of memory resources.

1) LITERATURE REVIEW

To provide reliable and realistic simulations in the 5G systems, existing channel models such as 3rd Generation Partnership Project (3GPP) Spatial Channel Model [5] and Wireless World Initiative New Radio (WINNER) [6] have been improved with new features such as mobility, spatial consistency, wide band support and spherical wave propagation, and also new models have been proposed [7]–[13].

Among the new models, COST 2100 [8], [14] is a geometry-based stochastic channel model (GBSCM) for frequency bands below 6 GHz. In this channel model, the characterization of different propagation conditions in the environment is introduced by dividing the clusters into three subgroups: single bounce-clusters, twin clusters, and local clusters. Many of these clusters are dispersed in the scenario at fixed locations from where parameters such as angles, delays and cluster powers are drawn from the geometry. To perform simulations with smooth time evolution and a non-stationary CIR, COST 2100 uses the concept of visibility region (VR). A VR is a two dimensional (2D) circular area in the scenario which defines the visibility of only one cluster, i.e., each cluster has its own VR. Therefore, when a user equipment (UE) moves through the scenario and pass by different VRs, it simulates the process of birth and death of clusters. Besides the frequency range limitation (below 6 GHz), COST 2100 does not support communication links with dual mobility such as V2V and D2D. Moreover, COST 2100 is widely characterized by the cluster parameters which are difficult to be obtained from measurements.

Quasi Deterministic Radio channel Generator (QuaDRiGa) [9] is an open source GBSCM which covers a large number of scenarios with single mobility for frequencies ranging from 0.45 GHz to 100 GHz and bandwidth up to 1 GHz. In QuaDRiGa, the correlated LSPs and the initial cluster parameters are generated using a stochastic approach [15] while the rays are drawn geometrically. QuaDRiGa also supports smooth time evolution with mobility by splitting the trajectory of the UEs into multiple segments and then interpolating the CIR of consecutive segments. This approach of smooth time evolution requires the prior knowledge of the trajectory for all UEs to ensure spatial consistency. However, despite the efforts to reduce the memory consumption required to generate correlated LSPs [15], the approach of time evolution used by QuaDRiGa still has a high memory consumption when simulations involving multi-user MIMO (MU-MIMO) systems with mobility are required and it is expected to be intractable for massive 5G networks, i.e., tens of base stations (BSs) and hundreds of UEs. Moreover, the correlated LSPs and SSPs experienced by a UE seen from different BSs are always uncorrelated even when the BSs are close to each other. This limitation will bring optimistic results for simulations in scenarios where the BSs are closely positioned.

To balance performance and computational complexity, Mobile and wireless communications Enablers for the Twenty-twenty Information Society (METIS) [10] project provided a stochastic channel model (SCM), a map-based channel model (MBCM) and also a hybrid model, by merging the SCM and MBCM. In the MBCM, many of the requirements for 5G channel modeling are present, such as specular reflection, diffuse scattering, blocking, diffraction, spherical wave propagations, smooth time evolution and spatial consistency for both single and dual mobility. In fact, this model allows high accurate simulations to evaluate many of the 5G

technologies, such as beamforming, mmWave, and massive MIMO. However, the computational complexity to compute the CIR in this model is still high since it is RT-based, mainly in outdoor environments, where the number of interacting objects is large. In contrast with the MBCM, the SCM proposed by METIS is less accurate and also demands a smaller complexity to compute the CIR. The SCM supports frequencies ranging up to 70 GHz and bandwidth up to 1 GHz. This model also supports single and dual mobility, but it still has many limitations such as no support for large antenna arrays and dynamic modeling. Moreover, the modeling for mmWave and spatial consistency are limited since the model only covers frequencies up to 70 GHz and the spatial consistency is restricted to the shadow fading (SF) which is obtained from a sum-of-sinusoids (SoS) method [16], such as in QuaDRiGa.

The 3GPP technical report (TR) 38.901 [13] describes an SCM and also an MBCM. Both models support frequencies ranging from 0.5 GHz to 100 GHz and bandwidth up to 2 GHz. As in METIS's models, the MBCM proposed by 3GPP leads to accurate simulations at the cost of high complexity while the SCM provides a better trade-off between accuracy and complexity. The 3GPP-SCM does not support communications with dual mobility but accounts for many of the 5G features for channel modeling. It has a WINNER-like core that can be used for simple drop-based simulations followed by the description of several additional modeling components such as blockage, oxygen absorption, spatial consistency, large bandwidth and also large antenna arrays. For simulations with large bandwidth and large arrays, the 3GPP-SCM assumes an individual time of arrival (ToA) and dynamic offset angles for each ray within a cluster, allowing to achieve high resolution in both delay and angular domains.

The number of rays per cluster in 3GPP-SCM is determined according to the scenario design and depends on the size of the antenna array, system bandwidth and per-cluster delay/angular spreads. The model describes two spatial consistency procedures, namely procedure-A and procedure-B. In procedure-A, the angles, delay, and power of each cluster are updated using linear approximations [17] based on the previous realization of each parameter while the rays have fixed delays and angle offsets. In procedure-B, the delay, angles, and power of clusters and rays are updated using spatially consistent random variables (SCRVs) obtained from a 2D-map. This procedure is recommended for simulations with large bandwidth and large arrays, but it requires many SCRVs and has a high memory consumption, as it will be shown in section IV-B.

International Mobile Telecommunications (IMT)-2020 [18] and Millimetre-Wave Based Mobile Radio Access Network for Fifth Generation Integrated Communications (mmMAGIC) [12] projects have proposed a GBSCM for communication with single mobility. The mmMAGIC model combines the stochastic approach from WINNER with the QuaDRiGa methodology to generate clusters to ensure a geometrical description. While the IMT-2020 model has adopted the 3GPP channel model for frequencies above 6 GHz as specified in [19] and the IMT-Advanced [20] channel model as a baseline. Both models cover a large frequency range and consider many of the 5G requirements for channel modeling.

Millimetre-Wave Evolution for Backhaul and Access (MiWEBA) [11] and IEEE 802.11ay [21] channel models support single and dual mobility communications but restricted to the frequency range from 57 GHz to 66 GHz and from 57 GHz to 68 GHz, respectively. Both models are based on a quasi-deterministic model which considers that deterministic rays contribute to almost all the power of the CIR and a few random rays are used to characterize reflections from surrounding objects. Both models have limited support for dynamic modeling and no support for high speed. Additionally, the IEEE 802.11ay channel model supports neither spatial consistency nor large arrays. Besides MiWEBA and IEEE 802.11ay, several channel models have been proposed for V2V communication [22]–[26], but they are quite limited in terms of 5G modeling components. In [27] a more sophisticated geometry-based model is proposed for both single and dual mobility but has no support for spatial consistency.

Besides the RT-based models MiWEBA, IEEE 802.11ay and METIS, several other RT-based models have been proposed for V2V communication [28], [29]. However, due to their high complexity [3], mainly for outdoor environments where the number of interacting objects is usually large, graphics processing units (GPUs) are required to make the modeling tractable. Finally, a more detailed review of channel models and measurements can be found in [30].

2) MAIN CONTRIBUTIONS

From the works found in the literature and discussed above, there are three main points which motivate the proposition of a new channel model:

1) The models that contain some 5G features for dual mobility are RT-based (e.g., MiWEBA, IEEE 802.11ay, and METIS) and demand a high computational complexity. Moreover, MiWEBA and IEEE 802.11ay only support a very restricted frequency range and limited dynamic modeling;
2) The GBSCMs and SCMs that generate correlated LSPs and SSPs individually for each BS (e.g., 3GPP, QuaDRiGa, and IMT-2020) will have too optimistic results for many 5G scenarios characterized by close proximity between the BSs, such as UDNs;
3) The SCMs that support dual mobility (e.g., METIS-SCM) are quite limited and only few 5G features are considered.

Given the limitations of existing channel models, the main contributions of this paper are listed below:

1) The proposed model—under the acronym 5G Stochastic Radio channel for dual Mobility (5G-StoRM)—is an extension of the 3GPP-SCM and supports dual mobility. Moreover, it has solved two of the main limitations in the 3GPP-SCM allowing efficient simulations in

many 5G scenarios, i.e., the number of SCRVs required to generate the CIR does not depend on the number of BSs deployed in the scenario and close BSs generate correlated LSPs and SSPs;
2) It offers a trade-off between computational complexity and accuracy while it keeps the overall consumed memory extremely low, even when challenging scenarios are considered, such as UDNs;
3) It has simplified the 3GPP procedure to generate the CIR allowing to remove some empirical coefficients employed in the 3GPP model;
4) To the best of the authors' knowledge, this is the first SCM that contains all the following 5G features: support for single and dual mobility with spatial consistency, smooth time evolution, dynamic modeling, large antenna array, frequency range up 100 GHz and bandwidth up to 2 GHz.

Finally, the remaining of the paper is organized as follows: section II describes a low complexity SoS-based procedure to generate SCRVs for single and dual mobility which will be widely used in the proposed channel model. Section III provides a detailed description of the proposed channel model. In section IV, the main calibration results are presented and compared with the baseline results. Finally, in section V, the conclusions of this work are presented.

II. SPATIALLY CORRELATED GAUSSIAN PROCESS GENERATION USING SoS Functions

In the proposed channel model, all of its stochastic parameters (e.g., LSPs, SSPs, line-of-sight (LOS)-to-non-line-of-sight (NLOS) transitions and O2I transitions) are characterized by a set of distributions which are modeled as SCRVs. In this context, this section describes a low computational complexity and also low memory consumption method to generate SCRVs for both single and dual mobility.

In [31], a method based on SoS functions is proposed to approximate a 2D spatially correlated Gaussian process with zero-mean and unit variance to model the SF for communication links with single mobility, i.e., either the transmitter (Tx) or receiver (Rx) moves. Assuming that, w.l.o.g., only the receiver moves, the Gaussian process approximation $\hat{\mathcal{N}}$ using a set $\mathbb{L} = \{1, 2, \ldots, L\}$ of cosine functions[1] is given by

$$\hat{\mathcal{N}}(\mathbf{c}_{\mathrm{Rx}}) = \sqrt{\frac{2}{L}} \sum_{l \in \mathbb{L}} \cos\left(2\pi (\mathbf{f}_{\mathrm{Rx},l})^{\mathrm{T}} \mathbf{c}_{\mathrm{Rx}} + \varphi_l\right), \tag{1}$$

where $\mathbf{c}_{\mathrm{Rx}} = \begin{bmatrix} x_{\mathrm{Rx}} & y_{\mathrm{Rx}} \end{bmatrix}^{\mathrm{T}}$ denotes the position of the Rx on the XY plane, $(\cdot)^{\mathrm{T}}$ is the transpose operation, φ_l is a random phase generated from the uniform distribution $\mathcal{U}$ as follows:

$$\varphi_l \sim \mathcal{U}(-\pi, \pi), \tag{2}$$

where $\mathbf{f}_{\mathrm{Rx},l} = \begin{bmatrix} f_{l,x} & f_{l,y} \end{bmatrix}^{\mathrm{T}}$ is the vector of spatial frequencies obtained from the autocorrelation function (ACF) $R_{\mathcal{N}}$ of the Gaussian process. $R_{\mathcal{N}}$ is typically modeled by an exponential function [6], [19], [32] as follows:

$$R_{\mathcal{N}}(\Delta\mathbf{c}_{\mathrm{Rx}}) = \exp\left(-\frac{\|\Delta\mathbf{c}_{\mathrm{Rx}}\|}{d_{\mathrm{cor}}}\right), \tag{3}$$

where $\Delta\mathbf{c}_{\mathrm{Rx}}$ is the receiver displacement, $\|\cdot\|$ is the Euclidean norm and d_{cor} is the decorrelation distance which is defined as the distance from where any two points of the SF process correlate equal to $\exp(-1) \approx 36.8\,\%$. In this context, the authors in [31] derived from the ACF in (3) a Monte Carlo sampling method to generate the spatial frequencies in (1) as follows:

$$\mathbf{f}_{\mathrm{Rx},l} = f_l \begin{bmatrix} \cos(\beta_l) & \sin(\beta_l) \end{bmatrix}^{\mathrm{T}}, \tag{4}$$

$$f_l = \frac{1}{2\pi d_{\mathrm{cor}}} \sqrt{\frac{1}{(1-U_l)^2} - 1}, \tag{5}$$

$$U_l \sim \mathcal{U}(0, 1) \text{ and } \beta_l \sim \mathcal{U}\left(-\frac{\pi}{2}, \frac{\pi}{2}\right). \tag{6}$$

In [33], the SoS presented above was generalized to also consider links with dual mobility. For this case, the ACF $R'_{\mathcal{N}}$ of the joint SF process is given by the product of two independent exponential ACFs as follows:

$$R'_{\mathcal{N}}(\Delta\mathbf{c}) = R_{\mathcal{N}}(\Delta\mathbf{c}_{\mathrm{Rx}}) R_{\mathcal{N}}(\Delta\mathbf{c}_{\mathrm{Tx}}), \tag{7}$$

where $\Delta\mathbf{c} = \begin{bmatrix} \Delta\mathbf{c}_{\mathrm{Tx}}{}^{\mathrm{T}} & \Delta\mathbf{c}_{\mathrm{Rx}}{}^{\mathrm{T}} \end{bmatrix}^{\mathrm{T}}$ is the joint displacement vector comprising both the transmitter and receiver displacements. The approximation to the SF process with dual mobility using the SoS coefficients is given by

$$\hat{\mathcal{N}}(\mathbf{c}) = \sqrt{\frac{2}{L}} \sum_{l \in \mathbb{L}} \cos\left(2\pi \mathbf{c}^{\mathrm{T}} \begin{bmatrix} \mathbf{f}_{\mathrm{Tx},l} \\ \mathbf{f}_{\mathrm{Rx},l} \end{bmatrix} + \varphi_l\right), \tag{8}$$

where $\mathbf{c} = \begin{bmatrix} \mathbf{c}_{\mathrm{Tx}}{}^{\mathrm{T}} & \mathbf{c}_{\mathrm{Rx}}{}^{\mathrm{T}} \end{bmatrix}^{\mathrm{T}}$ is the joint position vector, $\mathbf{f}_{\mathrm{Tx},l}$ and $\mathbf{f}_{\mathrm{Rx},l}$ correspond to the spatial frequencies associated with the transmitter and receiver, respectively, and are independently generated for both Tx and Rx according to (4)–(6) and φ_l is the random phase generated according to (2).

It is worth mentioning that the SoS method in (8) for dual mobility can also be used to generate SCRVs following different distributions by applying the corresponding transformation in the SF process. Such transformations are especially useful to generate the stochastic parameters of the proposed channel model which are not characterized by a normal distribution, such as angles and delays. In this context, using the error function erf(·), the zero-mean, unit variance SF process in (8) can be transformed into a uniform SCRV in the range [0, 1] as follows:

$$\hat{\mathcal{U}}(\mathbf{c}) = \frac{1}{2} + \frac{1}{2} \operatorname{erf}\left(\frac{\hat{\mathcal{N}}(\mathbf{c})}{\sqrt{2}}\right). \tag{9}$$

Also, using (9), an exponential SCRV (with unit mean and unit variance) and a Laplacian SCRV (with zero mean and unit variance) are obtained using the following transformations:

$$\hat{\mathcal{E}}(\mathbf{c}) = -\ln\left(\hat{\mathcal{U}}(\mathbf{c})\right), \tag{10}$$

[1] If not stated otherwise, throughout the paper the subscript l belongs to $\mathbb{L}$, i.e., $l \in \mathbb{L}$, where $\mathbb{L}$ is a set of L cosine functions used to generate a SCRV.

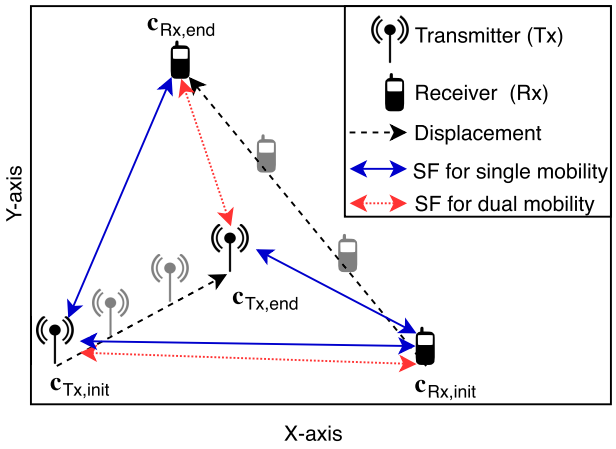

FIGURE 1. Communication link with single and dual mobility.

$$\hat{\mathcal{L}}(\mathbf{c}) = \frac{1}{\sqrt{2}} \ln\left(1 - 2\left|\hat{\mathcal{U}}(\mathbf{c}) - \frac{1}{2}\right|\right) \operatorname{sgn}\left(\hat{\mathcal{U}}(\mathbf{c}) - \frac{1}{2}\right), \quad (11)$$

respectively, where $\operatorname{sgn}(\cdot)$ is the signum function and $|\cdot|$ is the absolute value operator.

The scenario depicted in fig. 1 is used to exemplify how the SoS method in (8) is used to generate an SF process for both single and dual mobility. In this figure, the SoS method was applied for three configurations as follows:

1) Single mobility on the transmitter side (Tx-mobility): in this configuration, the receiver stays at the position $\mathbf{c}_{\text{Rx,init}}$ and the transmitter moves a distance equal to d_{cor} from the position $\mathbf{c}_{\text{Tx,init}}$ to $\mathbf{c}_{\text{Tx,end}}$;
2) Single mobility on the receiver side (Rx-mobility): in this configuration, the transmitter stays at the position $\mathbf{c}_{\text{Tx,init}}$ and the receiver moves a distance equal to $2d_{\text{cor}}$ from the position $\mathbf{c}_{\text{Rx,init}}$ to $\mathbf{c}_{\text{Rx,end}}$;
3) Dual mobility (Tx-Rx-mobility): in this configuration, both transmitter and receiver move, i.e., the transmitter moves from $\mathbf{c}_{\text{Tx,init}}$ to $\mathbf{c}_{\text{Tx,end}}$ and the receiver moves from $\mathbf{c}_{\text{Rx,init}}$ to $\mathbf{c}_{\text{Rx,end}}$.

Let d_{joint} be the normalized magnitude of the joint displacement vector $\Delta\mathbf{c}$ in (7), defined as

$$d_{\text{joint}} = \frac{\|\mathbf{c}_{\text{Tx,end}} - \mathbf{c}_{\text{Tx,init}}\| + \|\mathbf{c}_{\text{Rx,end}} - \mathbf{c}_{\text{Rx,init}}\|}{d_{\text{cor}}}. \quad (12)$$

In this context, for each configuration above, the generated SF process in (8) is depicted in fig. 2 versus d_{joint}. As it can be observed in this figure, when $d_{\text{joint}} = 0$, the generated SF is the same ($\approx -0.5\,\text{dB}$) for all configurations since they present the same starting point. Moreover, when d_{joint} increases, the SF changes smoothly and its fluctuations become different for each configuration since all the trajectories also present a different profile.

III. DESCRIPTION OF THE CHANNEL MODEL

5G-StoRM is an SCM that uses the SoS method described in section II to generate all of its stochastic parameters (i.e., LSPs and SSPs) and it has extended the 3GPP-SCM described

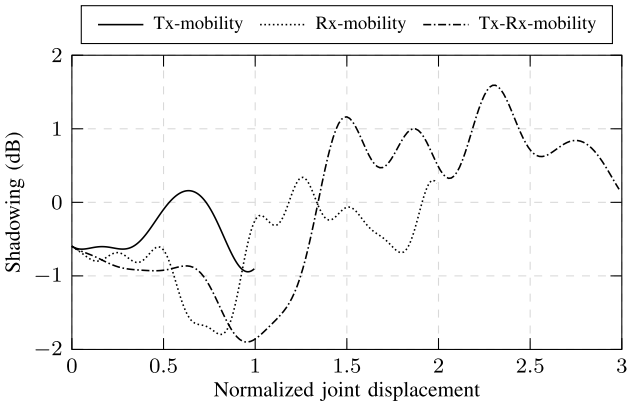

FIGURE 2. Spatially correlated SF for single and dual mobility using the generalized SoS method in (8).

in the TR 38.901 [13] by providing a spatially correlated CIR with smooth time evolution for communication links with single and dual mobility in a wide frequency range. Fig. 3 shows an overview of the steps to generate the channel coefficients.

A. CORRELATED LSPs

The angles, delay and power for each cluster are determined using seven LSPs:

1) shadow fading (SF);
2) Ricean K-factor (K);
3) delay spread (DS);
4) azimuth spread of departure (ASD);
5) azimuth spread of arrival (ASA);
6) zenith spread of departure (ZSD);
7) zenith spread of arrival (ZSA).

Each LSP $\tilde{\epsilon}_i, i \in \{\text{SF, K, DS, ASD, ASA, ZSD, ZSA}\}$, is generated in two steps. First, they are generated individually from a normal SCRV using the SoS method described in section II and correlated to each other using a 7×7 correlation matrix $\mathbf{R}$ as follows:

$$\begin{bmatrix} \tilde{\epsilon}_{\text{SF}} \\ \vdots \\ \tilde{\epsilon}_{\text{ZSA}} \end{bmatrix} = \begin{bmatrix} \mu_{\text{SF}} \\ \vdots \\ \mu_{\text{ZSA}} \end{bmatrix} + \begin{bmatrix} \sigma_{\text{SF}} & & \\ & \ddots & \\ & & \sigma_{\text{ZSA}} \end{bmatrix} \mathbf{R} \begin{bmatrix} z_1 \\ \vdots \\ z_7 \end{bmatrix}, \quad (13)$$

where $\mathbf{R}$, μ_i and σ_i, $i \in \{\text{SF, K, DS, ASD, ASA, ZSD, ZSA}\}$, are scenario-dependent configuration parameters loaded to the simulation in step (1) of the channel generation procedure depicted in fig. 3 and $z_i \sim \hat{\mathcal{N}}(\mathbf{c})$, $i = 1, \ldots, 7$. Next, the correlated LSPs in (13) are converted to linear scale as follows:

$$\epsilon_i = 10^{\tilde{\epsilon}_i}, \quad i \in \{\text{SF, K, DS, ASD, ASA, ZSD, ZSA}\}. \quad (14)$$

B. SETUP OF THE CLUSTERS

Some of the steps to generate the cluster's parameter in 5G-StoRM are different from the ones adopted by 3GPP. In the 3GPP-SCM, the delays are used to determine the power of the clusters while the angles of arrival and departure

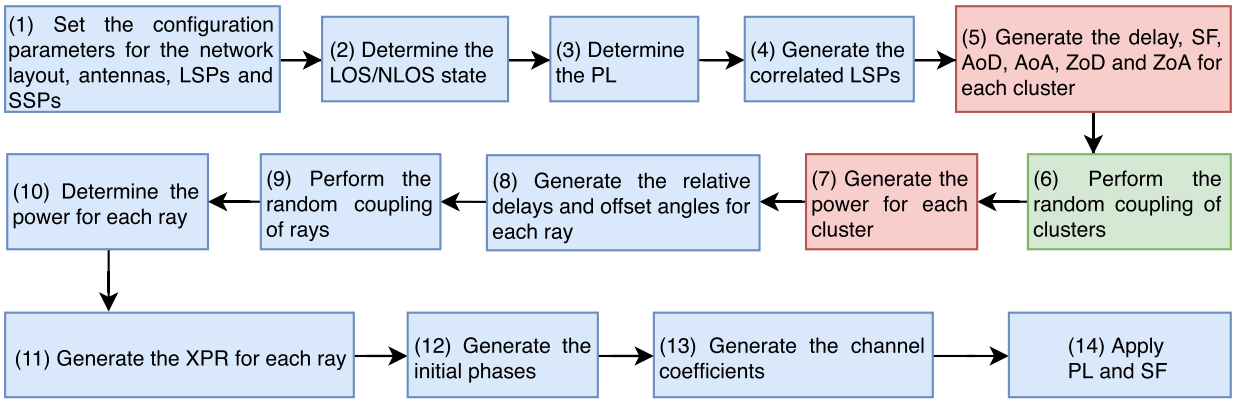

FIGURE 3. Steps to generate the channel coefficients. The steps (5) and (7) of the 3GPP model were changed in 5G-StoRM and also the step (6) was added to combine the changes in the 3GPP steps.

for both azimuth and zenith are obtained from the cluster power using empirical scaling factors [13, cf. pp. 34 and 35]. In 5G-StoRM, the delay and angles of each cluster are generated individually using the SoS method described in section II and then coupled randomly to form a cluster. After the coupling is performed, the power for each cluster is determined using its delay and angles. In this context, the delay of each cluster in 5G-StoRM is generated using an exponential SCRV as follows:

$$\tilde{\tau}_n = -r_\tau \epsilon_{\mathrm{DS}} X_n, \tag{15}$$

where r_τ is the empirical proportionality factor [6] used to correct the small delay spread generated by (15), ϵ_{DS} is the correlated DS from (14), $\mathbb{N} = \{1, 2, \ldots, N\}$ is the set of clusters[2] and $X_n \sim \hat{\mathcal{E}}(\mathbf{c})$. Next, the delays in (15) are normalized as follows:

$$\tau_n = \tilde{\tau}_n - \min\{\tilde{\tau}_1, \ldots, \tilde{\tau}_N\}. \tag{16}$$

The zenith angle of arrival (ZoA) and zenith angle of departure (ZoD) are generated as a wrapped Laplacian SCRV as follows:

$$\theta_n^{\mathrm{a}} = \arg\left\{\exp\left(j r_\tau \epsilon_{\mathrm{ZSA}} Y_n\right)\right\}, \tag{17}$$
$$\theta_n^{\mathrm{d}} = \arg\left\{\exp\left(j r_\tau \epsilon_{\mathrm{ZSD}} Z_n\right)\right\}, \tag{18}$$

respectively, where $\arg\{\cdot\}$ is the argument operator, ϵ_{ZSA} and ϵ_{ZSD} are the correlated ZSA and ZSD, respectively, determined in (14) and $(Y_n, Z_n) \sim \hat{\mathcal{L}}(\mathbf{c})$. In a similar manner, the azimuth angle of arrival (AoA) and azimuth angle of departure (AoD) are generated as a wrapped normal SCRV as follows:

$$\phi_n^{\mathrm{a}} = \arg\left\{\exp\left(j r_\tau \epsilon_{\mathrm{ASA}} W_n\right)\right\}, \tag{19}$$
$$\phi_n^{\mathrm{d}} = \arg\left\{\exp\left(j r_\tau \epsilon_{\mathrm{ASD}} G_n\right)\right\}, \tag{20}$$

respectively, where ϵ_{ASA} and ϵ_{ASD} correspond to the correlated ASA and ASD calculated in (14), respectively, and $(W_n, G_n) \sim \hat{\mathcal{N}}(\mathbf{c})$. Finally, the per-cluster SF is generated individually for each cluster as follows:

$$q_n = 10^{-\sigma_{\mathrm{cl}} \frac{Q_n}{10}}, \tag{21}$$

where $Q_n \sim \hat{\mathcal{N}}(\mathbf{c})$ and σ_{cl} corresponds to the standard deviation of the per-cluster SF. Next, the angles, delays, and SFs generated in (15)–(21) are coupled with the clusters, as shown in fig. 3 (step (6)). The coupling $\mathcal{C}_n$ consists in associating the cluster n with each one of its six parameters in (15)–(21). To this end, for each cluster n, the set of indices $\{n_i\}_{i=1}^6$ are chosen randomly such that

$$\mathcal{C}_n = \{\tau_{n_1}, \phi_{n_2}^{\mathrm{d}}, \phi_{n_3}^{\mathrm{a}}, \theta_{n_4}^{\mathrm{d}}, \theta_{n_5}^{\mathrm{a}}, q_{n_6}\}, \tag{22}$$
$$\mathcal{C}_q \cap \mathcal{C}_i = \emptyset, \quad \forall (q, i) \in \mathbb{N} \text{ and } q \neq i. \tag{23}$$

Note that constraint (23) ensures that each cluster has a unique set of indices $\{n_i\}_{i=1}^6$. In order to simplify the notation, w.l.o.g., it is assumed that the index of the cluster n matches the index of its six parameters, i.e.,

$$\mathcal{C}_n = \{\tau_n, \phi_n^{\mathrm{d}}, \phi_n^{\mathrm{a}}, \theta_n^{\mathrm{d}}, \theta_n^{\mathrm{a}}, q_n\}. \tag{24}$$

Finally, the power of each cluster is determined by the product of the individual probability density functions (PDFs) of the cluster delay and angles in (24) as follows:

$$\tilde{P}_n = \xi \exp\left(-\frac{\tau_n}{\frac{\sigma_{\mathrm{DS}}}{\eta_1}} - \frac{|\theta_n^{\mathrm{d}}|}{\frac{\sigma_{\mathrm{ZSD}}}{\eta_2\sqrt{2}}} - \frac{|\theta_n^{\mathrm{a}}|}{\frac{\sigma_{\mathrm{ZSA}}}{\eta_2\sqrt{2}}} - \frac{(\phi_n^{\mathrm{d}})^2}{2\frac{\sigma_{\mathrm{ASD}}^2}{\eta_3}} - \frac{(\phi_n^{\mathrm{a}})^2}{2\frac{\sigma_{\mathrm{ASD}}^2}{\eta_3}}\right) q_n, \tag{25}$$

where η_1, η_2 and η_3 are empirical factors proposed in [13, cf. section 7, (7.6.30b)–(7.6.30f)] to correct the small angular spread generated by this procedure due the wrapping performed over the angles in (17)–(20) and ξ is a positive constant. Next, the powers in (25) are normalized so that the

[2]If not stated otherwise, throughout the paper the subscript n belongs to $\mathbb{N}$, i.e., $n \in \mathbb{N}$, where $\mathbb{N}$ is a set of N clusters used to generate the CIR.

sum of all cluster powers is equal to one, i.e.,

$$P_n = \begin{cases} \dfrac{\tilde{P}_n}{\sum\limits_{n\in\mathbb{N}} \tilde{P}_n}, & \text{for NLOS,} \\ \dfrac{1}{\epsilon_{\mathrm{K}}+1}\dfrac{\tilde{P}_n}{\sum\limits_{n\in\mathbb{N}} \tilde{P}_n} + \delta(n-1)\dfrac{\epsilon_{\mathrm{K}}}{\epsilon_{\mathrm{K}}+1}, & \text{for LOS,} \end{cases} \tag{26}$$

where $n \in \mathbb{N}$ and $\delta(\cdot)$ is the Dirac delta function, ϵ_{K} is the correlated Ricean K-factor in (14) and the ratio $\epsilon_{\mathrm{K}}/(\epsilon_{\mathrm{K}}+1)$ corresponds to the power of the single LOS ray.

C. SETUP OF THE RAYS WITHIN A CLUSTER

Since many 5G scenarios employ massive MIMO and high bandwidth (larger than 1 GHz), realistic modeling of the rays within a cluster is required. To support realistic simulations in such scenarios, in 5G-StoRM the modeling described in the 3GPP channel model was assumed, i.e., each ray within a cluster has a unique delay, power and dynamic angles of arrival and departure for both azimuth and zenith. In this context, the relative delay of each ray $m \in \mathbb{M} = \{1, 2, \ldots, M\}$ with respect to the delay of its cluster $n \in \mathbb{N}$ is generated as a uniform SCRV[3] as follows:

$$\tilde{\tau}'_{n,m} = 2c_{\mathrm{DS}} X_{\mathrm{delay},n,m}, \tag{27}$$

where $X_{\mathrm{delay},n,m} \sim \hat{\mathcal{U}}(\mathbf{c})$, and c_{DS} is the scenario-dependent cluster DS. Next, the relative delays in (27) are normalized as follows:

$$\tilde{\tau}_{n,m} = \tilde{\tau}'_{n,m} - \min\{\tilde{\tau}'_{n,1}, \ldots, \tilde{\tau}'_{n,M}\}. \tag{28}$$

Following a similar procedure as in (27), the angles $\Phi^{\mathrm{a}}_{n,m}$, $\Phi^{\mathrm{d}}_{n,m}$, $\Theta^{\mathrm{a}}_{n,m}$ and $\Theta^{\mathrm{d}}_{n,m}$ which correspond, respectively, to the offset AoA, AoD, ZoA and ZoD angles of each ray $m \in \mathbb{M}$ within the cluster $n \in \mathbb{N}$ are generated from uniform SCRVs as follows:

$$\Phi^{\mathrm{d}}_{n,m} = 4X_{\mathrm{AoD},n,m} - 2 \text{ and } \Phi^{\mathrm{a}}_{n,m} = 4X_{\mathrm{AoA},n,m} - 2, \tag{29}$$

$$\Theta^{\mathrm{d}}_{n,m} = 4X_{\mathrm{ZoD},n,m} - 2 \text{ and } \Theta^{\mathrm{a}}_{n,m} = 4X_{\mathrm{ZoA},n,m} - 2, \tag{30}$$

where $X_{\mathrm{AoD/AoA/ZoD/ZoA},n,m} \sim \hat{\mathcal{U}}(\mathbf{c})$. Next, each ray m within the cluster n is coupled with its relative delay and offset angles specified in (28)–(30), i.e., the coupling of rays $\mathcal{R}_{n,m}$, $n \in \mathbb{N}$ and $m \in \mathbb{M}$, consists in selecting randomly the indices $\{m_i\}_{i=1}^{5}$ such that

$$\mathcal{R}_{n,m} = \{\tilde{\tau}_{n,m_1}, \Phi^{\mathrm{a}}_{n,m_2}, \Phi^{\mathrm{d}}_{n,m_3}, \Theta^{\mathrm{a}}_{n,m_4}, \Theta^{\mathrm{d}}_{n,m_5}\}, \tag{31}$$

$$\mathcal{R}_{n,q} \cap \mathcal{R}_{n,i} = \emptyset, \quad \forall (q,i) \in \mathbb{M} \text{ and } q \neq i. \tag{32}$$

Likewise in (23), (32) ensures that each ray within the cluster n has a unique set of indices. Moreover, w.l.o.g., it is assumed that the indices $\{m_i\}_{i=1}^{5}$ in (31) match the indices of the ray, i.e.,

$$\mathcal{R}_{n,m} = \{\tilde{\tau}_{n,m}, \Phi^{\mathrm{a}}_{n,m}, \Phi^{\mathrm{d}}_{n,m}, \Theta^{\mathrm{a}}_{n,m}, \Theta^{\mathrm{d}}_{n,m}\}. \tag{33}$$

[3]If not stated otherwise, throughout the paper the subscript m belongs to $\mathbb{M}$, i.e., $m \in \mathbb{M}$, where $\mathbb{M}$ is the set of M rays within each cluster $n \in \mathbb{N}$.

Based on that, the power of each ray is calculated as function of its parameters specified in (33) using an exponential mapping function, as follows:

$$\tilde{p}_{n,m} = \exp\left(-\frac{\tilde{\tau}_{n,m}}{c_{\mathrm{DS}}} - \frac{|\Phi^{\mathrm{d}}_{n,m}|}{\frac{c_{\mathrm{ASD}}}{\sqrt{2}}} - \frac{|\Phi^{\mathrm{a}}_{n,m}|}{\frac{c_{\mathrm{ASA}}}{\sqrt{2}}} - \frac{|\Theta^{\mathrm{d}}_{n,m}|}{\frac{c_{\mathrm{ZSD}}}{\sqrt{2}}} - \frac{|\Theta^{\mathrm{a}}_{n,m}|}{\frac{c_{\mathrm{ZSA}}}{\sqrt{2}}}\right), \tag{34}$$

where $c_{\mathrm{ASD/ASA/ZSD/ZSA}}$ corresponds to the scenario-dependent cluster angular spreads for both azimuth and zenith. Next, the power of the rays in (34) is normalized so that the sum of their powers is equal to the power of the cluster they belong to, i.e.,

$$p_{n,m} = P_n \frac{\tilde{p}_{n,m}}{\sum\limits_{m\in\mathbb{M}} \tilde{p}_{n,m}}. \tag{35}$$

Finally, from the coupling of clusters in (24) and the coupling of rays in (33), it is possible to determine the angles and delay for each ray $m \in \mathbb{M}$, within each cluster $n \in \mathbb{N}$, as follows:

$$\tau_{n,m} = \tau_{\mathrm{LOS}} + \eta_{\mathrm{delay}}\tau_n + \tilde{\tau}_{n,m}, \tag{36}$$

$$\phi^{\mathrm{d}}_{n,m} = \phi^{\mathrm{d}}_{\mathrm{LOS}} + \eta_{\mathrm{angle}}\phi^{\mathrm{d}}_n + c_{\mathrm{ASD}}\Phi^{\mathrm{d}}_{n,m}, \tag{37}$$

$$\phi^{\mathrm{a}}_{n,m} = \phi^{\mathrm{a}}_{\mathrm{LOS}} + \eta_{\mathrm{angle}}\phi^{\mathrm{a}}_n + c_{\mathrm{ASA}}\Phi^{\mathrm{a}}_{n,m}, \tag{38}$$

$$\theta^{\mathrm{d}}_{n,m} = \theta^{\mathrm{d}}_{\mathrm{LOS}} + \eta_{\mathrm{angle}}\theta^{\mathrm{d}}_n + c_{\mathrm{ZSD}}\Theta^{\mathrm{d}}_{n,m}, \tag{39}$$

$$\theta^{\mathrm{a}}_{n,m} = \theta^{\mathrm{a}}_{\mathrm{LOS}} + \eta_{\mathrm{angle}}\theta^{\mathrm{a}}_n + c_{\mathrm{ZSA}}\Theta^{\mathrm{d}}_{n,m}, \tag{40}$$

where τ_{LOS}, $\phi^{\mathrm{d}}_{\mathrm{LOS}}$, $\phi^{\mathrm{a}}_{\mathrm{LOS}}$, $\theta^{\mathrm{d}}_{\mathrm{LOS}}$ and $\theta^{\mathrm{a}}_{\mathrm{LOS}}$ represent the delay, the AoD, the AoA, the ZoD and the ZoA of the single LOS ray, respectively, η_{delay} and η_{angle} are empirical scaling factors used to correct the delay and angular spreads generated for this procedure when there is LOS, i.e., $\eta_{\mathrm{delay}} = \eta_{\mathrm{angle}} = 1$ for NLOS and $\eta_{\mathrm{delay}} = \sqrt{1 + (\epsilon_{\mathrm{K}}/2)}$ and $\eta_{\mathrm{angle}} = \sqrt{1+\epsilon_{\mathrm{K}}}$ [13, cf. section 7.6] for LOS.

D. ANTENNA MODELING AND XPR

The antenna array modeling in 5G-StoRM was designed to support three main realistic antenna effects [13, cf. sections 7.1 and 7.3 (model-2)]:

1) 3D rotations;
2) Single-linear and cross-linear polarization;
3) Directive radiation power pattern (RPP).

Such effects are combined to generate the antenna element (AE) response $\mathbf{a}$ expressed in spherical coordinates with respect to the wavefront vector $\mathbf{r}$ as follows:

$$\mathbf{a} = \overbrace{\mathbf{F}}^{\text{Rotation}} \overbrace{\begin{bmatrix} \cos(\psi) & 0 \\ 0 & \sin(\psi) \end{bmatrix}}^{\text{Polarization}} \overbrace{\sqrt{R(\mathbf{r})}}^{\text{RPP}} \exp\left(\frac{2\pi j}{\lambda}\mathbf{r}^{\mathrm{T}}\mathbf{d}\right), \tag{41}$$

where $\mathbf{r}$ corresponds to the pair of angles θ (zenith) and ϕ (azimuth) transformed to Cartesian coordinates as follows

$$\mathbf{r} = \begin{bmatrix} \sin(\theta)\cos(\phi) & \sin(\theta)\sin(\phi) & \cos(\theta) \end{bmatrix}^{\mathrm{T}}, \tag{42}$$

d is a 3D vector that points from the reference point of the antenna array to the position of the AE, λ is the wavelength, $R(\cdot)$ represents the directive RPP of the AE, ψ is the polarization angle and **F** describes 3D rotations.

In order to model the losses due to cross-polarization power ratio (XPR) of the NLOS rays while propagating from the transmitter to the receiver, 5G-StoRM uses the same approach as in [6], [13], i.e., a 2×2 rotation matrix **X** combines the AE responses of transmitter and receiver as

$$A_{u,s,n,m} = (\mathbf{a}_{\mathrm{Rx},u,n,m})^{\mathrm{T}} \mathbf{X} (\mathbf{a}_{\mathrm{Tx},s,n,m}), \tag{43}$$

where $\mathbf{a}_{\mathrm{Tx},s,n,m}$ and $\mathbf{a}_{\mathrm{Rx},u,n,m}$ are the response of the AE s and u of the transmitter and receiver, respectively, with respect to the ray m within the cluster n. The matrix **X** is given by

$$\mathbf{X} = \begin{cases} \begin{bmatrix} 1 & 0 \\ 0 & -1 \end{bmatrix} \exp\left(-2\pi j \frac{\|\mathbf{c}_{\mathrm{Tx}} - \mathbf{c}_{\mathrm{Rx}}\|}{\lambda}\right), & \text{LOS ray,} \\ \begin{bmatrix} \exp\left(j\Omega_{n,m}^{\mathrm{VV}}\right) & \frac{\exp\left(j\Omega_{n,m}^{\mathrm{VH}}\right)}{\sqrt{\kappa_{n,m}}} \\ \frac{\exp\left(j\Omega_{n,m}^{\mathrm{HV}}\right)}{\sqrt{\kappa_{n,m}}} & \exp\left(j\Omega_{n,m}^{\mathrm{HH}}\right) \end{bmatrix}, & \text{otherwise,} \end{cases} \tag{44}$$

where $\Omega_{n,m}^{\mathrm{VV}}$, $\Omega_{n,m}^{\mathrm{VH}}$, $\Omega_{n,m}^{\mathrm{HV}}$ and $\Omega_{n,m}^{\mathrm{HH}}$ are random phases independently generated for each ray as a uniform SCRV in (9) in the range $(-\pi, \pi]$ and $\kappa_{n,m}$ is the XPR coefficient which quantifies the polarization changes of the transmitted field through the propagation path for each ray. $\kappa_{n,m}$ is generated independently for each ray as a lognormal SCRV, i.e., $\kappa_{n,m} = 10^{\mu_{\mathrm{XPR}} + \sigma_{\mathrm{XPR}} z_{n,m}}$, where μ_{XPR} and σ_{XPR} are the scenario-dependent mean and standard deviation of the XPR, both expressed in dB, and $z_{n,m} \sim \hat{\mathcal{N}}(\mathbf{c})$. Finally, note that there is no change of polarization to the LOS ray since it does not suffer reflections or diffractions.

E. CHANNEL IMPULSE RESPONSE

The CIR is generated by combining the angles, delay and power of each ray in (35)–(40) with the antenna patterns in (43) as follows:

$$\begin{aligned} h_{u,s}\left(\mathcal{T}_{q,b}\right) &= \sqrt{\frac{g}{\epsilon_{\mathrm{K}}+1}} \sum_{\substack{n\in\mathbb{N} \\ m\in\mathbb{M}}} \left(\sqrt{p_{n,m}}\, A_{u,s,n,m}\, d_{n,m}(t) \delta\left(\tau - \tau_{n,m}\right)\right) \\ &\quad + \sqrt{\frac{g\epsilon_{\mathrm{K}}}{\epsilon_{\mathrm{K}}+1}} A_{u,s,\mathrm{LOS}}\, d_{\mathrm{LOS}}(t) \delta\left(\tau - \tau_{\mathrm{LOS}}\right), \end{aligned} \tag{45}$$

where $\mathcal{T}_{q,b} \triangleq \{\mathbf{c}_{q,b}, t, \tau\}$ is the domain of the CIR, i.e., it is composed of time domain t, the delay domain τ and the space domain $\mathbf{c}_{q,b}$ which represents the joint position vector that is composed of the transmitter antenna b and the receiver antenna q, s and u denote the index of the AE in the transmitter antenna b and the receiver antenna q, respectively, g is the large scale gain which comprises the path loss (PL), the penetration building loss (for O2I) and the SF in (14), ϵ_{K} is the Ricean K-factor also generated in (14), $A_{u,s,\mathrm{LOS}}$ denotes the combined antenna patterns in (43) for the LOS ray and $d_{n,m}$ quantifies the joint Doppler shift defined as

$$d_{n,m}(t) = \exp\left(\frac{2\pi j}{\lambda}\left((\mathbf{v}_b)^{\mathrm{T}} \mathbf{r}_{b,n,m} + (\mathbf{v}_q)^{\mathrm{T}} \mathbf{r}_{q,n,m}\right)\right), \tag{46}$$

where $\mathbf{v}_b$ and $\mathbf{v}_q$ represent the 3D velocity of the antenna b and antenna q, respectively. Finally, d_{LOS} in (45), represents the joint Doppler shift due to the LOS ray which is also determined using (46) by replacing the multi-path wavefronts by the LOS wavefront.

TABLE 1. Calibration metrics.

Group	Metric
Large bandwidth and large antenna arrays	Cumulative distribution function (CDF) of the 1st singular value
Spatial consistency	Cross-correlation coefficient (CCC) of the CIR vs. distance
LSP	CDF of the coupling loss (CL) and signal to interference plus noise ratio (SINR)
SSP	CDF of the DS, ASA and ZSD

IV. NUMERICAL RESULTS AND CHANNEL CALIBRATION

This section presents numerical simulations showing some of the advantages of 5G-StoRM over existing channel models. Also, it presents the calibration of the proposed channel model using the results reported by 19 companies in the scenarios urban macro (UMa), urban micro (UMi) and indoor for different frequencies. It is worth mentioning that this section covers only the single mobility case since neither the calibration results nor the scenario-dependent parameters that are available in the literature include scenarios with dual mobility.

The configuration of each scenario (e.g., all the scenario-dependent parameters, the scenario layout, etc.) is specified in [32] and the calibration results reported by the companies are available on the 3GPP website [34]–[36]. Since many results were reported, four groups of calibration results were chosen to be reproduced using 5G-StoRM. The selected groups and the calibration metrics for each group are summarized in table 1. The two first calibration groups aim to show that 5G-StoRM supports some of the main features for channel modeling in 5G systems while the last two groups aim to show the correctness of the proposed model. In this context, the first groups in table 1 will be discussed in this section, while the last two groups are discussed in appendices V-A and V-B.

Moreover, for each metric in table 1, the 19 curves provided by 3GPP were replaced by an area-plot, i.e., such results are plotted as a filled area, which correspond to the smallest area (boundary) that contains all the curves provided by 3GPP. As such, if a calibrated result using 5G-StoRM falls within that area, it means this result is in concordance with

TABLE 2. Main simulation parameters from [32, cf. tables 7.8-1, 7.8-2 and 7.8-4] to perform the channel calibration.

		Group			
		Large band. and large ant. arrays	Spatial consistency	LSP	SSP
Parameter	Scenarios	UMi		UMa, UMi and indoor	
	Scenario layout	Hexagon grid for UMa and UMi composed of 19 BSs, and rectangular grid for indoor composed by 12 BSs			
	System frequency	30 GHz		6, 30 and 70 GHz	
	Bandwidth	2 GHz	100 MHz	20 MHz for 6 GHz and 100 MHz above 6 GHz	
	BS sectorization	3 sectors per BS			
	BS transmit power	35 dBm for UMa and UMi above 6 GHz. 49 dBm and 44 dBm at 6 GHz for UMa and UMi, respectively, and 24 dBm for indoor in all frequencies			
	BS antenna pol.	Cross-polarized (45 and −45 deg)		Vertical	Cross-polarized (45 and −45 deg)
	BS antenna config.	4 URAs each one with 8 × 8 AEs	2 URAs each one with 4 × 4 AEs	Single ULA with 10 AEs	2 URAs each one with 4 × 4 AEs
	BS ant. port mapping	All the AEs for each polarization on each ULA and each URA are mapped to a single cell-specific reference signal (CRS) port			
	UE antenna pol.	Cross-polarized (0 and 90 deg)		Vertical	Cross-polarized (0 and 90 deg)
	UE placement	Uniform for indoor scenario. For UMa and UMi the UE dropping is described in [19, cf. table 6.1]			
	UE antenna config.	Single AE with isotropic radiation power pattern			
	N. of rays per cluster	40	20		
	UE attachment	Based on the RSRP obtained from antenna port 0 (fast fading is enabled)		Based on the single LOS ray (fast fading is disabled)	Based on the RSRP obtained from antenna port 0 (fast fading is enabled)

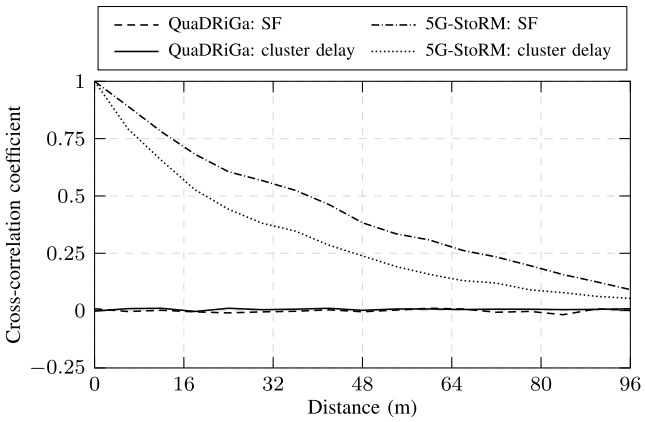

FIGURE 4. CCCs of SF and delay of 3rd cluster versus distance between two BSs, using 5G-StoRM and QuaDRiGa. The considered scenario is UMa-NLOS specified in [32, cf. Table 7.5-6] and system frequency of 6 GHz.

3GPP calibrations. Finally, the main simulation parameters for all calibrations are depicted in table 2.

A. CORRELATED LSPs AND SSPs FOR CLOSE BSs

As previously mentioned, in 5G-StoRM, close BSs generate correlated LSPs and SSPs since they share common clusters. To evaluate this feature in 5G-StoRM, the open-source channel model QuaDRiGa was chosen for comparison purposes. The simulated scenario comprises a fixed UE and two BSs (i.e., BS_1 and BS_2). The two BSs—initially co-localized—move in opposite directions following a straight trajectory. Let D be the distance between the two BSs ranging from 0 m to 95 m. Hence, the CCC $\rho_{SF}(D)$ of the SF ϵ_{SF} of link BS_1-UE with the SF ϵ'_{SF} of link BS_2-UE is given by

$$\rho_{SF}(D) = \frac{E\left[\epsilon_{SF}\epsilon'_{SF}\right] - E\left[\epsilon_{SF}\right]E\left[\epsilon'_{SF}\right]}{\sqrt{E\left[\epsilon^2_{SF}\right]E\left[\epsilon'^2_{SF}\right]}}, \tag{47}$$

where $E[\cdot]$ denotes the expectation operator. In a similar manner, the CCC $\rho_{\tau_3}(D)$ of the third cluster delay τ_3 of link BS_1-UE with the third cluster delay of link BS_2-UE is also calculated using (47) by replacing ϵ_{SF} by τ_3 and ϵ'_{SF} by τ'_3, respectively.[4]

Fig. 4 shows the aforementioned CCCs versus distance D. As it can be observed, in 5G-StoRM, both coefficients decay smoothly, showing that the fading processes of the two links are highly-correlated. Moreover, the decaying rate of such CCCs in fig. 4 is characterized by the decorrelation distance described in section II, which is scenario-dependent and can be found in [32, cf. Table 7.5-6]. On the other hand, when the QuaDRiGa channel model is considered, both CCCs obtained from (47) are approximately zero for any distance D. This limitation in QuaDRiGa (and also in the 3GPP-SCM model) provides optimist results (e.g., in terms of system capacity) in many 5G scenarios characterized by the presence of close BSs, such as UDNs [4].

B. MEMORY REQUIREMENTS AND COMPUTATIONAL COMPLEXITY

The amount of computational resources, i.e., memory and processing, spent to construct an SCM is vastly dependent

[4] With exception of the first cluster, which has its delay normalized to zero, any of the other clusters will provide the same CCC, since they are generated as a i.i.d. SCRV.

on the number of SCRVs used to generate its CIR and also the procedure used to generate them. The grid-based and filtering methods [9] store each SCRV as a grid of points equally spaced in XY-plane that covers all the simulated scenario. Both methods allow fast channel calculations by interpolating four points from a lookup table. However, they do not support dual mobility and demand large memory consumption (described in the next paragraphs). In this context, it will be compared the required memory to generate all the SCRVs in a UMa scenario for 5G-StoRM and the 3GPP-SCM. Since 3GPP-SCM only supports single mobility and does not specify its procedure to generate SCRVs, it will be assumed the grid-based method and the SoS method for single mobility described in section II.

To represent an SCRV, the SoS methods for single mobility in (1) and dual mobility in (8) require the storage of $3L$ and $5L$ real numbers, respectively; while the grid-based method stores $\lceil S_{\text{UMa}}/d_{\text{cor}} \rceil^2$ real numbers, where S_{UMa} is the size of the considered UMa squared layout and $\lceil x \rceil$ denotes the largest integer smaller than x.

In addition, to a given scenario, the number of SCRVs required by 5G-StoRM to compute the CIR in (45) is directly determined from the channel generation procedure described in section III: each LSP in (13) is characterized by one SCRV; each cluster requires six SCRVs as shown in (17)–(21),, i.e., four for angles of arrival and departure, one for delay and one for SF; and each ray within a cluster requires ten SCRVs as shown in (27), (29), (30) and (44), i.e, one for the relative delay, four for the offset angles, four for the initial phases and one for the XPR. Therefore, 5G-StoRM requires, approximately, a total of

$$N' = \begin{cases} 7 + 6N + 10NM, & \text{for indoor and O2O,} \\ (7 + 6N + 10NM)N_{\text{f}}, & \text{for O2I,} \end{cases} \tag{48}$$

SCRVs to generate the CIR, where N_{f} is the number of floors in the O2I scenario, i.e., the SCRVs are generated independently for each floor, since they are assumed to be uncorrelated [13].

Finally, combining the storage needs discussed above with (48), the amount of real numbers demanded by 5G-StoRM and 3GPP-SCM to compute the CIR in (45) is given by

$$\tilde{N}_{\text{StoRM}} = 5LN', \tag{49}$$

$$\tilde{N}_{\text{3GPP}} = \begin{cases} 3LN_{\text{BS}}N', & \text{for SoS single mobility,} \\ \left\lceil \dfrac{S_{\text{UMa}}}{d_{\text{cor}}} \right\rceil^2 N_{\text{BS}}N', & \text{for grid-based,} \end{cases} \tag{50}$$

where N_{BS} denotes the number of BSs deployed in the scenario, i.e., all the SCRVs are generated individually for each BS in the 3GPP-SCM.

Fig. 5 shows the required memory by 5G-StoRM and 3GPP-SCM versus the number of BSs deployed in a UMa scenario for a different number of rays per cluster. To plot the curves, it was assumed that each real number in (49) and (50) is expressed in single precision, i.e., it requires four bytes.

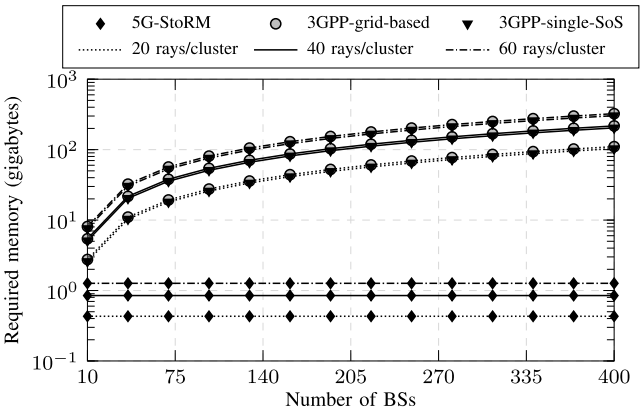

FIGURE 5. Required memory to generate the set of SCRVs in a full-UMa scenario, i.e., there are communication links O2O (LOS and NLOS) and also O2I (LOS and NLOS), simultaneously. It was used $L = 500$ SoS coefficients, $d_{\text{cor}} = 50$ meter and $S_{\text{UMa}} = 2$ km.

As it can be observed in fig. 5, both strategies used to generate the SCRVs in the 3GPP-SCM present a limited capability to simulate scenarios with more than 10 BSs due to its high memory demand. For simulations with 100 BSs, the memory required by 3GPP model using the methods in (50) is around 28, 50 and 85 gigabytes for 20, 40 and 60 rays per cluster, respectively. For simulations with massive MIMO and large bandwidth, the number of rays per cluster can be larger than 60 which brings practical limitations in the 3GPP model. Furthermore, challenging scenarios such as UDNs are expected in 5G systems. In this case, when 400 BSs are deployed in the system, 3GPP-SCM requires between 100 and 300 gigabytes to store all the SCRVs while 5G-StoRM does not require more than 1.5 gigabytes.

Considering the analyzed scenario in fig. 5, the 5G-StoRM needs to compute L cosine functions to determine any stochastic parameter in (45), while the grid-based method only needs to interpolate four points from a lookup table. This means that 5G-StoRM demands a computational complexity which increases linearly with L and it is L times higher than the grid-based method. One may consider as a disadvantage of the proposed model over the 3GPP model. However, note that $300 \leq L \leq 500$ is enough to provide good accuracy in the SoS method [33]. Thus, this justifies why 5G-StoRM can still be considered of low complexity.

At last, although 5G-StoRM may provide a less accurate channel response than RT-based models, the proposed model—and any stochastic one—turns out to be much less complex, specially in outdoor dense networks such as UDNs [4].

C. CALIBRATION FOR LARGE BANDWIDTH AND LARGE ANTENNA ARRAYS

This calibration analyzes the fast fading fluctuations around the average channel power through eigenvalue decomposition (EVD) of the channel matrix in the frequency domain.

For this purpose, the scenario is configured according to table 2, i.e., each sector of a BS (from now on, named as BS-sector) is equipped with four uniform rectangular arrays (URAs) 8 × 8 cross-polarized and each UE has a single isotropic AE, which is also cross-polarized. The system bandwidth is 2 GHz and 40 rays per cluster were used in order to achieve a high resolution in delay and angular domains.

Let $\mathbb{Q} = \{1, 2, \ldots, Q\}$ and $\mathbb{B} = \{1, 2, \ldots, B\}$ be the sets of UEs and BS-sectors deployed in the scenario, respectively. For each BS-sector, the received and transmitted signals on each URA for each polarization are virtualized to a single antenna port, resulting in eight ports. The reference signal received power (RSRP) from antenna port 0 is used as criterion to define connection between each UE $q \in \mathbb{Q}$ and its serving BS-sector $b' \in \mathbb{B}$ in three steps: first, the RSRP from antenna port 0 between the UE q and each BS-sector is determined as [19, cf. section 8] follows:

$$\mathrm{RSRP}_{q,b} = \frac{P_{\mathrm{T}}}{N_{\mathrm{U}}} \int_0^{\infty} \left(\sum_{u=1}^{N_{\mathrm{U}}} \left| \sum_{s=1}^{S} h_{u,s} \left(\mathcal{T}_{q,b} \right) \right|^2 \right) \mathrm{d}\tau, \quad (51)$$

where $N_{\mathrm{U}} = 2$ is the number of virtual AEs on each UE, i.e., a single AE dual-polarized, $S = 64$ is the number of virtual AEs that comprises the antenna port 0 on each BS-sector and P_{T} is the BS-sector transmitted power, in Watt, defined in table 2. Next, each UE $q \in \mathbb{Q}$ is connected with the BS-sector b' that provides the largest RSRP, i.e.,

$$b'(q) = \arg\max_{b \in \mathbb{B}} \left\{ \mathrm{RSRP}_{q,1}, \ldots, \mathrm{RSRP}_{q,B} \right\}, \quad q \in \mathbb{Q}. \quad (52)$$

Finally, the vector of singular values $\mathbf{v} = \left[v_1^2 \; v_2^2 \right]^{\mathrm{T}}$ is obtained from the virtualized channel matrix $\mathbf{H}$, in the frequency domain, for a physical resource block (PRB) within the considered bandwidth, using the eigenvalue decomposition EVD(·), as follows:

$$\mathbf{v} = \mathrm{EVD} \left(\frac{\mathbf{H}\mathbf{H}^{\mathrm{H}}}{g} \right), \quad (53)$$

where g is the overall large scale gain defined in (45) and $(\cdot)^{\mathrm{H}}$ denotes the conjugate transpose operation. Note that $\mathbf{H}$ has dimensions 2 × 8 since each UE has a single AE dual-polarized and each BS-sector has four panels also dual-polarized.

In this context, the CDF of the 1st singular value v_1^2, expressed in dB, is depicted in fig. 6. As it can be observed from this figure, the received power of a transmitted data stream using this eigenmode fluctuates from −10 dB to 30 dB around the large scale gain g. Moreover, most of the CDF is above 0 dB due to the high array gain obtained from the directive AEs that comprise each panel [32, cf. table 7.1-3], showing why massive MIMO systems are widely used in literature to combat the frequency-dependent path loss and also frequency-selective channels in mmWave. Finally, from fig. 6, the reader may notice that calibration using 5G-StoRM agree well with the 3GPP curves.

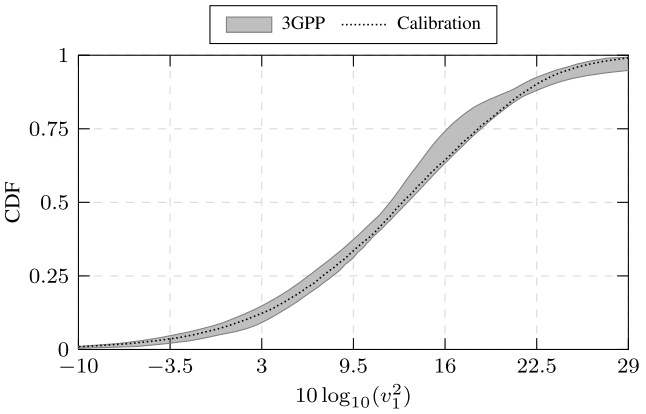

FIGURE 6. CDF of the 1st singular value of the channel matrix for UMi scenario at 30 GHz.

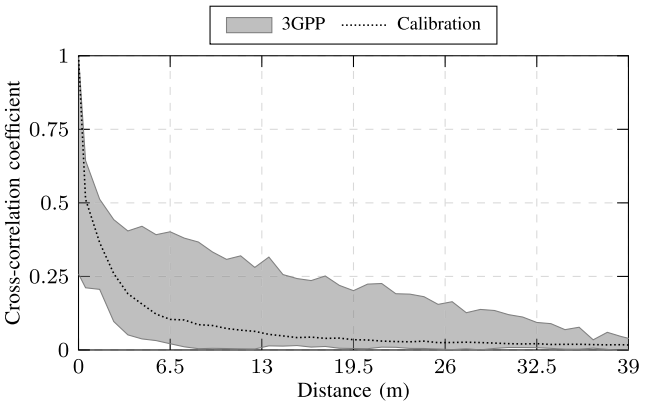

FIGURE 7. Cross-correlation coefficient of the CIR vs. the distance for UMi scenario at 30 GHz.

D. CALIBRATION FOR SPATIAL CONSISTENCY

As shown in table 2, for this calibration, there is a single BS composed of three BS-sectors. Each BS-sector is equipped with two URAs 4 × 4 cross-polarized and the UEs have a single isotropic AE, also cross-polarized. In this context, the calibration was done in two steps: firstly, two UEs are placed randomly around the BS separated by a fixed distance $D \in \mathbb{D} = \{0, 0.5, 1, \ldots, 40\}$, in meter, and then the serving BS-sector $b' \in \mathbb{B} = \{1, 2, 3\}$ for each UE $q \in \mathbb{Q} = \{1, 2\}$ is determined according to (51). Next, the cross-correlation coefficient between the CIR of each UE was calculated as follows:

$$\rho(D) = \left| \frac{\mathrm{E}[H_1 H_2^*] - \mathrm{E}[H_1]\,\mathrm{E}[H_2^*]}{\sqrt{\mathrm{E}[H_1 H_1^*]\,\mathrm{E}[H_2 H_2^*]}} \right|, \quad (54)$$

where H_q, $q \in \{1, 2\}$, is the CIR in the frequency domain between the first AE of the UE q and the first AE of its serving BS-sector and $(\cdot)^*$ is the conjugate complex operator.

Fig. 7 depicts the cross-correlation coefficient defined in (54) versus the separation distance between the UEs. One can see a good agreement between the 5G-StoRM and the 3GPP results. Still in this figure, one can also observe a large variation of the area-plot in the results reported by 3GPP.

For instance, when $D = 0$ m, ρ ranges from 0.25 to 1. For $\rho = 0.36$, D ranges from 0 m to 7.5 m. Some implementation details that are left open in the 3GPP TR 38901 [13], such as initial phases of rays, might explain this large variation. That is, the initial phases of each ray in (44) can be generated using different approaches, e.g., as SCRVs or i.i.d. random variables and each one yields different levels of correlation.

V. CONCLUSIONS AND FUTURE WORKS

In this paper, a new channel model was proposed for 5G systems under the acronym 5G-StoRM. By means of the SoS method to generate SCRVs, the proposed model has extended the 3GPP-SCM by considering three main features: support for dual mobility, spatial correlation at both ends of the communication link and a considerable reduction of the required memory when compared with other channel models.

The problem of uncorrelated LSPs and SSPs from close BSs that is present in 3GPP-SCM, QuaDRiGa, IMT-2020 and METIS-SCM, was solved in 5G-StoRM allowing more realistic simulations in many 5G scenarios, characterized by a large density of BSs and UEs per unit of area, such as UDNs, indoor environments, D2D and V2V.

To the best of authors' knowledge, the proposed model is the first SCM, and therein low-complexity when compared with RT-based models, which contains all the following 5G features: support for single and dual mobility with spatial consistency, smooth time evolution, dynamic modeling, large antenna array, frequency range up 100 GHz and bandwidth up to 2 GHz. Moreover, some of these features were calibrated in the scenarios UMa, UMi and indoor and have shown a good agreement with the results reported by 19 companies.

For future works, there are some points which can be investigated:

- The SoS method used in 5G-StoRM can be generalized to consider mobility also in the vertical direction (Z-axis) allowing the model to also support air-to-everything (A2X) links. To this end, the description of LSPs and SSPs using the SoS method for dual mobility should be characterized by measurements (or RT-based simulations) assuming mobility in the vertical direction. Note that buildings, scattering, etc., present a different distribution through the horizontal and vertical planes, which means that LSPs and SSPs may present a different behavior when the transmitter and receiver move in the Z-axis;
- Some new features can also be added to the model, such as spherical wave propagation, oxygen absorption, ground reflection, and blockers. Spherical waves feature is the most challenging one because it requires the physical location of clusters, while 5G-StoRM was developed using a fully stochastic approach. In this context, a stochastic modeling based on SoS method for dual mobility could be an attractive solution to describe the physical location of clusters due to its low memory consumption requirement.

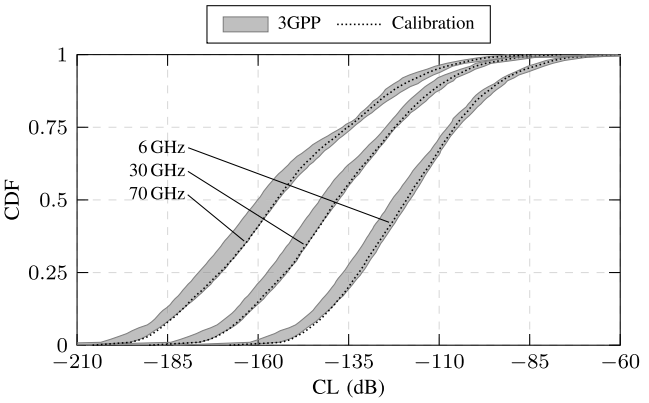

FIGURE 8. CDF of the CL for UMa scenario.

APPENDIX
ADDITIONAL CALIBRATIONS

For completeness, this appendix resumes section IV with the calibration results of LSPs and SSPs.

A. CALIBRATIONS OF LSPs

As it is shown in table 2, each BS-sector is equipped with a uniform linear array (ULA) composed of 10 AEs and the UE has a single AE, both vertically polarized. The first LSP metric to be evaluated is the CL, which is defined as the strongest signal strength received on each UE from all BS-sectors in the system. In this context, let $\mathbb{B} = \{1, \ldots, B\}$ and $\mathbb{Q} = \{1, \ldots, Q\}$ be the sets of BS-sectors and UEs deployed in the system, respectively. The strength $\Upsilon_{b,q}$ of the received signal between the BS-sector $b \in \mathbb{B}$ and the UE $q \in \mathbb{Q}$ is then given by

$$\Upsilon_{q,b} = \sum_{s=1}^{10} \left| h_{1,s}\left(\mathcal{T}_{q,b}\right) \right|^2, \tag{55}$$

where $h_{u,s}$ is the CIR in (45) evaluated only for the single LOS ray, i.e., $\mathcal{T}_{q,b} = \{\mathbf{c}_{q,b}, 0, \tau_{\text{LOS}}\}$. Finally, the coupling loss CL_q of each UE $q \in \mathbb{Q}$ is obtained from (55) as follows:

$$\text{CL}_q = \max\{\Upsilon_{q,1}, \ldots, \Upsilon_{q,B}\}, \quad q \in \mathbb{Q}. \tag{56}$$

The 5G-StoRM calibrations of the CL for UMa, UMi, and indoor are shown in figs. 8–10, respectively. For all these curves, the CL values in the right tail of the CDF correspond to the UEs which are close to the BS under LOS. Similarly, the CL values in the left tail of the CDF corresponds to the UEs in the boundary of adjacent cells and are in NLOS. Also, in these figures, it is noted a considerable frequency-dependent CL. It can be observed in 50th percentile of each CDF, when the overall loss has increased around 40 dB and 20 dB from 6 GHz to 70 GHz for UMa/UMi and indoor scenarios, respectively. In comparison with the CL of the three scenarios depicted in figs. 8–10 for each frequency, it is noted that the scenarios UMa and UMi experience an overall loss larger than 50 dB with respect to the indoor scenario. This large loss is a composition of two main factors: 1) the indoor scenario is most comprised by LOS

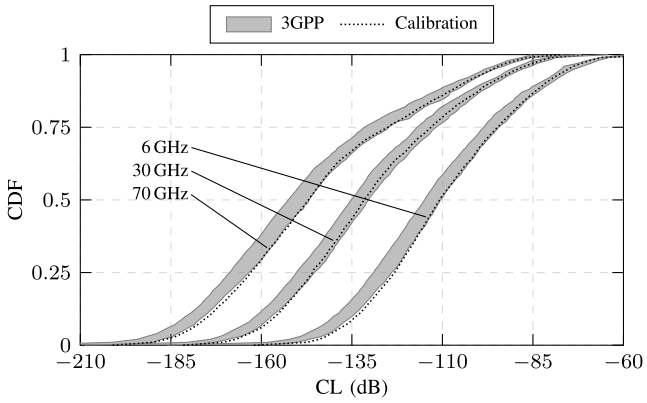

FIGURE 9. CDF of the CL for UMi scenario.

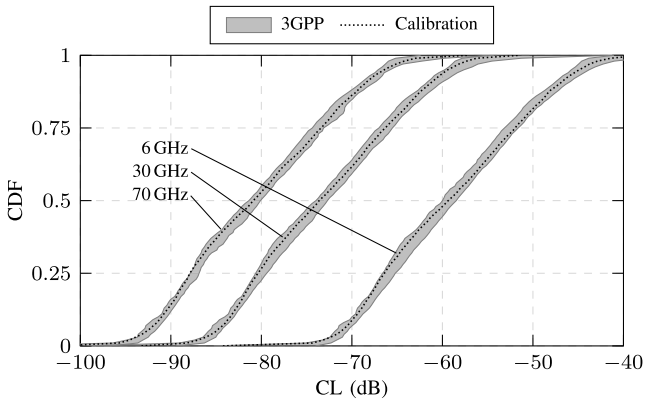

FIGURE 10. CDF of the CL for indoor scenario.

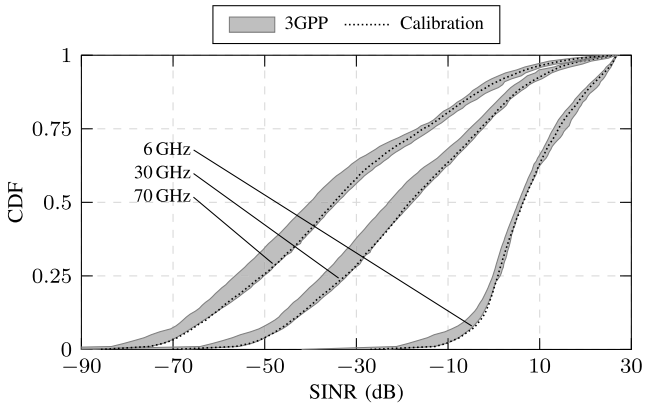

FIGURE 11. CDF of the SINR for UMa scenario.

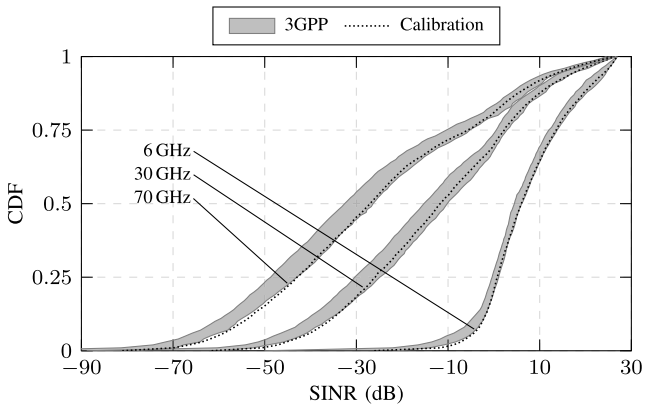

FIGURE 12. CDF of the SINR for UMi scenario.

due to the small distance between adjacent BSs, while the scenarios UMa and UMi are most characterized by NLOS propagation, and 2) 80% of the UEs in the scenarios UMa and UMi are indoor and experience a large frequency-dependent building loss.

Besides the calibration of the CL, the calibration of the SINR provides a more detailed characterization of each scenario since it considers some additional parameters, such as transmitted power, noise power, and system bandwidth. For this calibration, the SINR for each UE $q \in \mathbb{Q}$ is determined using its CL in (56) as follows:

$$\mathrm{SINR}_q = \frac{\mathrm{CL}_q}{\eta + \sum\limits_{b \in \mathbb{B}} \Upsilon_{b,q} - \mathrm{CL}_q}, \quad q \in \mathbb{Q}, \tag{57}$$

where η is the ratio between the noise power in the system bandwidth and the BS-sector transmitted power. In this context, the calibration of the SINR using 5G-StoRM in the scenarios UMa, UMi and indoor are depicted in figs. 11–13, respectively. Analyzing figs. 11 and 12, it is noted very poor SINR conditions around the 50th percentile of the CDF for UMa and UMi at 30 and 70 GHz, while it stays in good conditions at 6 GHz for both scenarios. It happens due to three reasons: 1) the high frequency-dependent CL shown in figs. 8 and 9; 2) from table 2, it is possible to see that the system bandwidth at 6 GHz is five times smaller than the system bandwidth in 30 and 70 GHz and 3) the transmitted power at 6 GHz is 14 and 9 dBm larger than the transmitted power above 6 GHz for UMa and UMi, respectively. Hence, the scenarios UMa and UMi are mainly limited by interference at 6 GHz and by noise above 6 GHz. Now, analyzing fig. 13, it is noted that the SINR for indoor scenario is almost the same for all frequencies. It happens because the interference term in (57) is much larger than the noise term η, which characterizes a scenario limited by interference. Finally, it is noted that all calibrated LSPs metrics using 5G-StoRM, depicted in figs. 8–13, are in accordance with 3GPP results.

B. CALIBRATION OF SSPs

As it is shown in table 2, each BS-sector in the scenario is equipped with two URAs 4 × 4 with cross-polarized AEs, and the UEs have a single cross-polarized isotropic AE. To perform the SSP calibrations, each UE $q \in \mathbb{Q}$ is connected with the BS-sector that provides the strongest RSRP from antenna port 0, as expressed in (52). After the connection is established, the different SSP calibrations presented in table 1 are performed. The first SSP calibration to be analyzed is the DS, given by

$$\sigma_\tau = \sqrt{\sum_{\substack{n \in \mathbb{N} \\ m \in \mathbb{M}}} p_{n,m} \tau_{n,m}^2 - \left(\sum_{\substack{n \in \mathbb{N} \\ m \in \mathbb{M}}} p_{n,m} \tau_{n,m} \right)^2}, \tag{58}$$

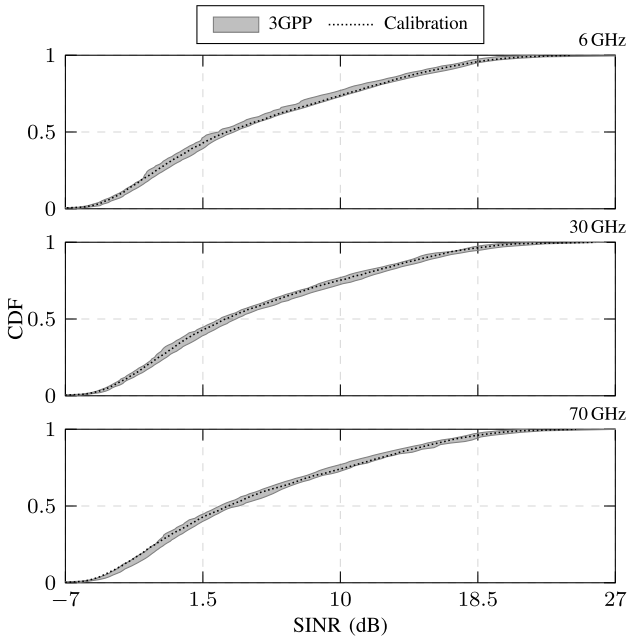

FIGURE 13. CDF of the SINR for indoor scenario.

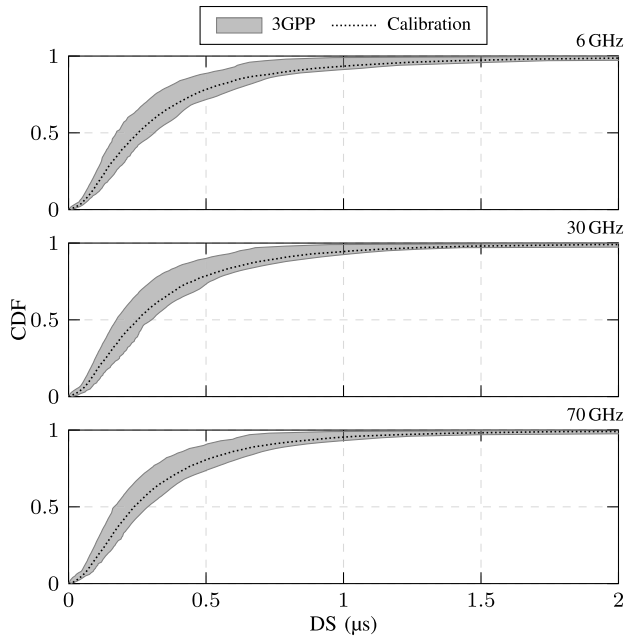

FIGURE 14. CDF of the DS for UMa scenario.

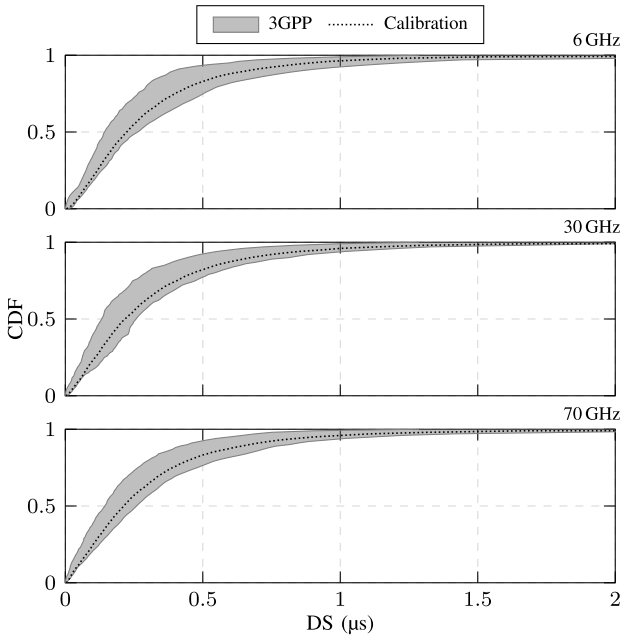

FIGURE 15. CDF of the DS for UMi scenario.

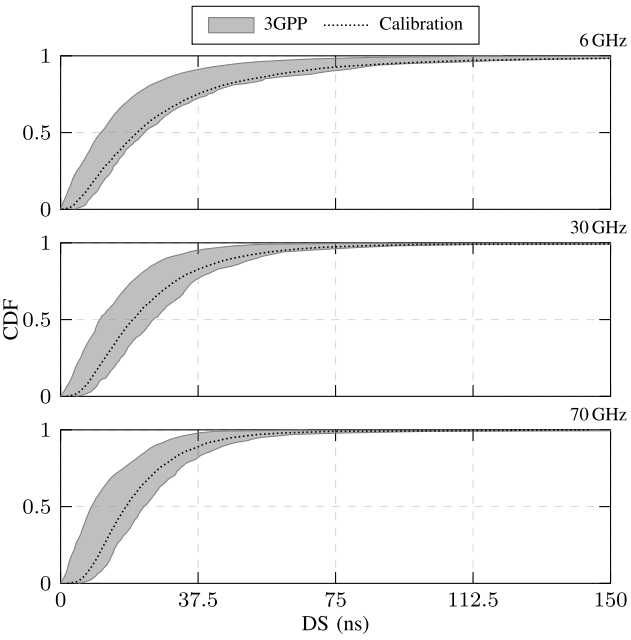

FIGURE 16. CDF of the DS for indoor scenario.

and its CDF is depicted in figs. 14–16 for different frequencies in UMa, UMi and indoor scenarios, respectively. The CDFs for UMa and UMi presented in figs. 14 and 15 are 80% composed of O2I links which do not have frequency-dependent LSPs [32, cf. table 7.5-6]. As a consequence of that, the only difference between such CDFs comes from the 20% remaining O2O links which are characterized by frequency-dependent LSPs. On the other hand, the CDFs of the DS for indoor scenario presented in fig. 16 are most composed of links under LOS conditions due to small distance between BSs and UEs and have slightly frequency-dependent LSPs [32, cf. table 7.5-6].

The second metric to be evaluated for SSP calibrations is the CDF of the ZSD. The ZSD is determined according to the circular angle spread presented in [5, cf. pp. 39]. Its CDFs for different frequencies in UMa, UMi, and indoor scenarios are depicted in figs. 17–19, respectively. As it can be noted, the CDF of the ZSD for UMa and UMi scenarios in figs. 17 and 18, respectively, are almost the same for all frequencies. In fact, the ZSD for UMa and UMi scenar-

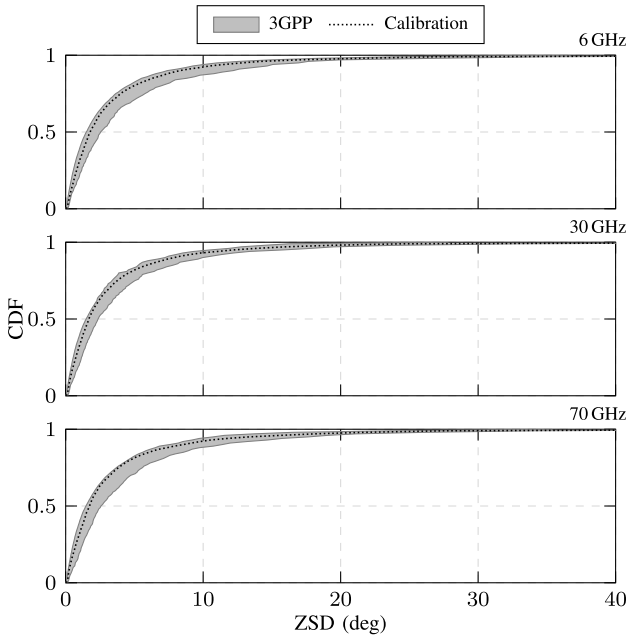

FIGURE 17. CDF of the ZSD for UMa scenario.

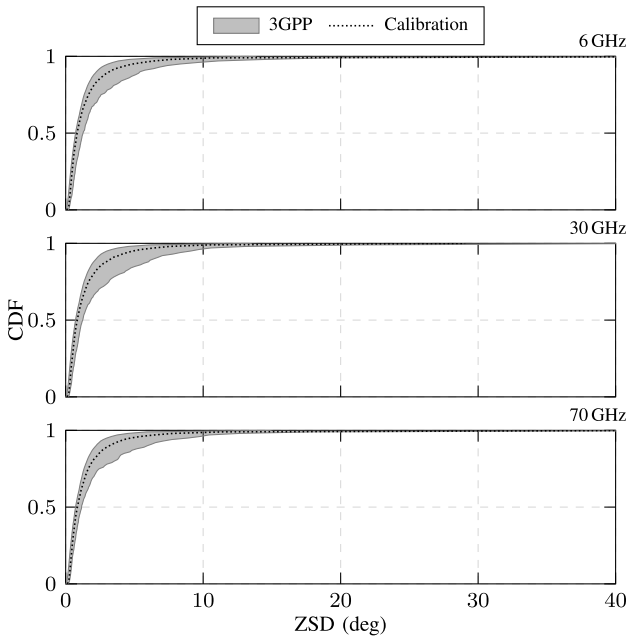

FIGURE 18. CDF of the ZSD for UMi scenario.

ios is mostly characterized by the difference between the BS's and UE's heights and the 2D distance between them rather than system frequency [32, cf. tables 7.5-7 and 7.5-8]. On the other hand, the CDF of the ZSD for indoor scenario, depicted in fig. 19, has a considerable dependence on the system frequency [32, cf. table 7.5-10]. Finally, from figs. 14–19 is noted that there is a good agreement between all SSP calibrations using 5G-StoRM and the results reported by 3GPP.

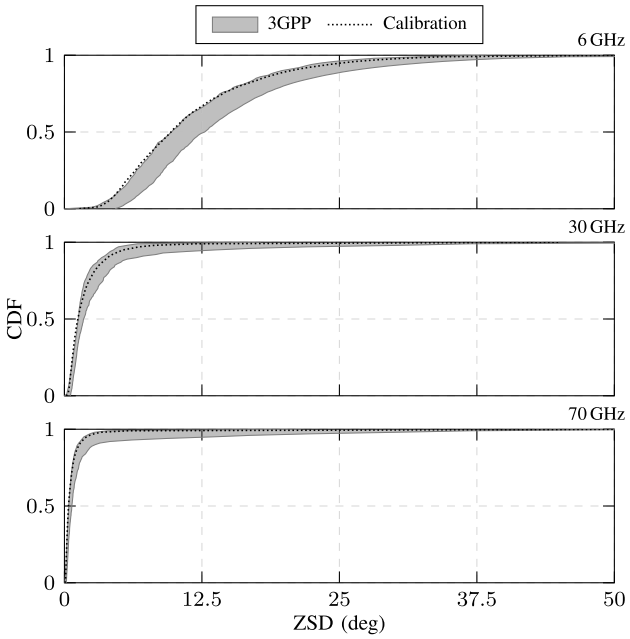

FIGURE 19. CDF of the ZSD for indoor scenario.

REFERENCES

[1] *Cisco Visual Networking Index: Forecast and Methodology*, Cisco, San Jose, CA, USA, Jun. 2017.

[2] J. G. Andrews, S. Buzzi, W. Choi, S. V. Hanly, A. Lozano, A. C. K. Soong, and J. C. Zhang, "What will 5G be?" *IEEE J. Sel. Areas Commun.*, vol. 32, no. 6, pp. 1065–1082, Jun. 2014.

[3] Z. Yun and M. F. Iskander, "Ray tracing for radio propagation modeling: Principles and applications," *IEEE Access*, vol. 3, pp. 1089–1100, 2015.

[4] M. Kamel, W. Hamouda, and A. Youssef, "Ultra-dense networks: A survey," *IEEE Commun. Surveys Tuts.*, vol. 18, no. 4, pp. 2522–2545, 4th Quart., 2016.

[5] *Spatial Channel Model for Multiple Input Multiple Output (MIMO) Simulations*, document TR 25.996, 3GPP, Jun. 2018.

[6] P. Kyösti *et al.*, "WINNER II channel models, V1.2," WINNER, Deliverable 1.1.2, Tech. Rep., Sep. 2007.

[7] S. Sun, G. R. MacCartney, and T. S. Rappaport, "A novel millimeter-wave channel simulator and applications for 5G wireless communications," in *Proc. IEEE Int. Conf. Commun. (ICC)*, May 2017, pp. 1–7.

[8] K. Haneda, J. Poutanen, F. Tuvfesson, L. Liu, V. Kolmonen, P. Vainikainen, and C. Oestges, "Development of multi-link geometry-based stochastic channel models," in *Proc. Loughborough Antennas Propag. Conf.*, Nov. 2011, pp. 1–7.

[9] S. Jaeckel, L. Raschkowski, L. Thiele, F. Burkhardt, and E. Eberlein, *Quadriga Quasi Determinisc Radio Channel Generator, User Manual and Documentation*, document v1.2.3-307, 2017.

[10] V. Nurmela *et al.*, "METIS channel models," METIS, Deliverable 1.4, Tech. Rep., Jul. 2015.

[11] A. Maltsev *et al.*, "Channel modeling and characterization," MiWEBA, Deliverable 5.1, Tech. Rep., Jun. 2014.

[12] K. Haneda *et al.*, "Measurement results and final mmMAGIC channel models," mmMAGIC, Deliverable 2.2, Tech. Rep., May 2017.

[13] *Study on Channel Model for Frequencies From 0.5 to 100 GHz*, document ETSI TR 138 901 V14.0.0, 3GPP, Jun. 2018.

[14] L. Liu, C. Oestges, J. Poutanen, K. Haneda, P. Vainikainen, F. Quitin, F. Tufvesson, and P. D. Doncker, "The COST 2100 MIMO channel model," *IEEE Wireless Commun.*, vol. 19, no. 6, pp. 92–99, Dec. 2012.

[15] M. Kurras, S. Dai, S. Jaeckel, and L. Thiele. (Aug. 2018). *Evaluation of the Spatial Consistency Feature in the 3GPP GSCM Channel Model*. [Online]. Available: https://www.researchgate.net/publication/326989772_Evaluation_of_the_Spatial_Consistency_Feature_in_the_3GPP_GSCM_Channel_Model

[16] T. Jämsä and P. Kyösti, "Device-to-device extension to geometry-based stochastic channel models," in *Proc. 9th Eur. Conf. Antennas Propag. (EuCAP)*, Apr. 2015, pp. 1–4.

[17] Y. Wang, L. Huang, Z. Shi, K. Liu, and X. Zou, "A millimeter wave channel model with variant angles under 3GPP SCM framework," in *Proc. IEEE 26th Annu. Int. Symp. Pers., Indoor, Mobile Radio Commun. (PIMRC)*, Aug./Sep. 2015, pp. 2249–2254.
[18] *Draft New Report ITU-R M.[IMT-2020.EVAL]—Guidelines for Evaluation of Radio Interface Technologies for IMT-2020*, document ITU-R SG05, ITU-R, 2017.
[19] *Study on 3D Channel Model for LTE*, document 36.873, 3GPP, Jan. 2018.
[20] *Guidelines for Evaluation of Radio Interface Technologies for IMT-Advanced*, document M.2135, ITU-R, Dec. 2009.
[21] A. Maltsev, A. Pudeyev, A. Lomayev, and I. Bolotin, "Channel modeling in the next generation mmWave Wi-Fi: IEEE 802.11ay standard," in *Proc. 22nd Eur. Wireless Conf.*, 2016, pp. 1–8.
[22] A. Chelli and M. Patzold, "The impact of fixed and moving scatterers on the statistics of MIMO vehicle-to-vehicle channels," in *Proc. IEEE 69th Veh. Technol. Conf. (VTC-Spring)*, Apr. 2009, pp. 1–6.
[23] A. G. Zajić, G. L. Stuber, T. G. Pratt, and S. T. Nguyen, "Wideband MIMO mobile-to-mobile channels: Geometry-based statistical modeling with experimental verification," *IEEE Trans. Veh. Technol.*, vol. 58, no. 2, pp. 517–534, Feb. 2009.
[24] Y. Yuan, C.-X. Wang, X. Cheng, B. Ai, and D. I. Laurenson, "Novel 3D geometry-based stochastic models for non-isotropic MIMO vehicle-to-vehicle channels," *IEEE Trans. Wireless Commun.*, vol. 13, no. 1, pp. 298–309, Jan. 2014.
[25] Y. Yuan, C.-X. Wang, Y. He, M. M. Alwakeel, and E. M. Aggoune, "3D wideband non-stationary geometry-based stochastic models for non-isotropic MIMO vehicle-to-vehicle channels," *IEEE Trans. Wireless Commun.*, vol. 14, no. 12, pp. 6883–6895, Dec. 2015.
[26] S. Yoo and K. Kim, "An improved temporal correlation model for vehicle-to-vehicle channels with moving scatterers," in *Proc. URSI Asia–Pacific Radio Sci. Conf. (URSI AP-RASC)*, Aug. 2016, pp. 1391–1392.
[27] S. Wu, C.-X. Wang, E.-H. M. Aggoune, M. M. Alwakeel, and X. You, "A general 3-D non-stationary 5G wireless channel model," *IEEE Trans. Commun.*, vol. 66, no. 7, pp. 3065–3078, Jul. 2018.
[28] J. Maurer, T. Fugen, and W. Wiesbeck, "Physical layer simulations of IEEE 802.11a for vehicle-to-vehicle communications," in *Proc. IEEE 62nd Veh. Technol. Conf. (VTC-Fall)*, vol. 3, Sep. 2005, pp. 1849–1853.
[29] W. Wiesbeck and S. Knorzer, "Characteristics of the mobile channel for high velocities," in *Proc. Int. Conf. Electromagn. Adv. Appl.*, Sep. 2007, pp. 116–120.
[30] C.-X. Wang, J. Bian, J. Sun, W. Zhang, and M. Zhang, "A survey of 5G channel measurements and models," *IEEE Commun. Surveys Tuts.*, vol. 20, no. 4, pp. 3142–3168, 4th Quart., 2018.
[31] X. Cai and G. B. Giannakis, "A two-dimensional channel simulation model for shadowing processes," *IEEE Trans. Veh. Technol.*, vol. 52, no. 6, pp. 1558–1567, Nov. 2003.
[32] *Study on Channel Model for Frequency Spectrum Above 6 GHz*, document ETSI TR 138 900 V14.2.0, 3GPP, Jul. 2016.
[33] Z. Wang, E. K. Tameh, and A. R. Nix, "Joint shadowing process in urban peer-to-peer radio channels," *IEEE Trans. Veh. Technol.*, vol. 57, no. 1, pp. 52–64, Jan. 2008.
[34] *E-Mail Discussion Summary of the Large Scale Calibration*, document 3GPP TSG RAN WG1 #85, Jun. 2016.
[35] *E-Mail Discussion Summary of the Full Scale Calibration*, document 3GPP TSG RAN WG1 #85, Jun. 2016.
[36] *E-Mail Discussion Summary [87–35] on Additional Feature Calibration*, document R1-1709900, 3GPP TSG RAN WG1-NR, 3rd Generation Partnership Project (3GPP), Jan. 2017.

ALEXANDRE M. PESSOA received the B.Sc. and M.Sc. degrees in computer engineering from the Federal University of Ceará (UFC), Sobral, Brazil, in 2015 and 2017, respectively, where he is currently pursuing the D.Sc. degree in teleinformatics with a focus on systems and communication networks. Since 2014, he has been a Collaborator and a Researcher with the Wireless Telecom Research Group (GTEL), UFC, where he has been involved in the project Remote area Access Network for 5G GEneration (5G-RANGE) in cooperation with universities/institutes from Brazil and Europe. His research interests include radio resource allocation for spectrum sensing techniques and channel modeling for 5G systems.

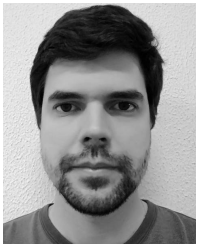

IGOR M. GUERREIRO received the B.S., M.S., and Ph.D. degrees in teleinformatics engineering from the Federal University of Ceará (UFC), Brazil, in 2007, 2010, and 2016, respectively.

He currently holds a postdoctoral position at the Department of Teleinformatics Engineering, UFC. Since 2007, he has been a Researcher with the Wireless Telecom Research Group (GTEL), Brazil, working in research projects within a technical cooperation with Ericsson Research, Sweden. In 2008, he was a Guest Researcher with the Virginia Tech Advanced Research Institute (ARI), Arlington, VA, USA. Before starting the Ph.D. course at UFC, he visited Ericsson, Luleå, Sweden, in 2010, for five months, and then Ericsson, San Jose, CA, USA, for three months. As a Ph.D. student, he visited Ericsson and the Royal Institute of Technology (KTH), Stockholm, Sweden, from 2014 to 2015, for a year-long period. His research interests include techniques for MIMO transceiver design, strategies for distributed optimization for wireless communication systems, modeling and simulation of cellular communication, vehicular communication, machine learning for wireless communications, graph signal processing, dynamic spectrum access methodologies, and physical layer aspects for the Internet of Things.

CARLOS F. M. E. SILVA received the five-year Diploma degree and M.Sc. degrees in electronics and telecommunications engineering from the University of Aveiro (UA), Portugal, in 2005 and 2010, respectively, and the Ph.D. degree in teleinformatics engineering from the Federal University of Ceará (UFC), Brazil, in 2015. Since 2006, he has been a Researcher in several European projects, such as WINNER II (system requirements for beyond third-generation wireless networks), FUTON (RRM for wireless and optical networks), and COGEU (cognitive radio systems for efficient use and sharing of TVWS in the European context). He currently holds a postdoctoral position with the Wireless Telecom Research Group (GTEL), Brazil, where he manages GTEL's team in the European–Brazilian project FUTEBOL and also works in cooperation projects with Ericsson Research. His main research interests include spectrum usage optimization, TV white spaces, licensed shared access, the Internet of Things, device-to-device communications, test bed experimentation, and architectural aspects of the future 5G networks.

TARCISIO F. MACIEL received the B.Sc. and M.Sc. degrees in electrical engineering from the Federal University of Ceará (UFC), in 2002 and 2004, respectively, and the Dr.Ing. degree in electrical engineering from the Technische Universität Darmstadt (TUD), Germany, in 2008. Since 2001, he has actively participated in several projects in a technical and scientific cooperation between the Wireless Telecom Research Group (GTEL), UFC, and Ericsson Research. From 2005 to 2008, he was a Research Assistant with the Communications Engineering Laboratory, TUD. Since 2008, he has been a member of the Postgraduation Program in Teleinformatics Enginnering, UFC. In 2009, he was a Professor of computer engineering with UFC-Sobral. Since 2010, he has been a Professor with the Center of Technology, UFC. His research interests include radio resource management, numerical optimization, and multiuser/multiantenna communications.

DIEGO A. SOUSA received the B.Sc. degree in computer engineering from the University of Ceará (UFC), Sobral, Brazil, in 2011, and the M.Sc. and Ph.D. degrees in teleinformatics engineering from UFC, Fortaleza, Brazil, in 2013 and 2018, respectively. Since 2013, he has been a Researcher with the Wireless Telecom Research Group (GTEL), UFC, participating of projects in a technical and scientific cooperation with Ericsson Research. Since 2013, he has been a Professor with the Federal Institute of Education, Science, and Technology of Ceará (IFCE), Paracuru, Brazil. His research interests include numerical optimization, 5G networks, coordinated scheduling, and radio resource allocation for QoS/QoE provisioning.

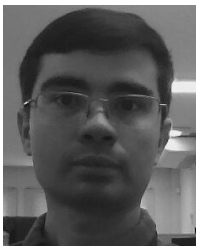

DARLAN C. MOREIRA received the bachelor's degree in electrical engineering and the M.Sc. degree in teleinformatics from the Federal University of Ceará (UFC), in 2005 and 2007, respectively. He is currently a member of the Wireless Telecom Research Group (GTEL), Fortaleza, Brazil, where he has been working in projects within the technical cooperation between GTEL and Ericsson Research for more than ten years. His research interests include MIMO-OFDM, dynamic TDD and V2X communications, and 5G systems in general.

FRANCISCO R. P. CAVALCANTI received the B.Sc. and M.Sc. degrees in electrical engineering from the Federal University of Ceará (UFC), Fortaleza, Brazil, in 1994 and 1996, respectively, and the D.Sc. Degree in Electrical Engineering from the State University of Campinas, Campinas, Brazil, in 1999. He then joined the UFC, where he is currently an Associate Professor and the Wireless Communications Chair with the Department of Teleinformatics Engineering. In 2000, he founded and, since then, has directed the Wireless Telecom Research Group (GTEL), which is a research laboratory based in Fortaleza, which focuses on the advancement of wireless telecommunications technologies. At GTEL, he manages a 20-year-long program of research projects in wireless communications sponsored by Ericsson Research, Brazil and Sweden. He has produced a varied body of work, including two edited books, conference and journal articles, international patents, and computer software dealing with subjects such as radio resource allocation, cross-layer algorithms, quality-of-service provisioning, radio transceiver architectures, signal processing, and project management. He is also a Distinguished Researcher of the Brazilian Scientific and Technological Development Council for his technology development and innovation record. He also holds a Leadership and Management Professional Certificate from the Massachusetts Institute of Technology, Cambridge.